NRL Report 7899



# The NRL Fluid-Cooled Helix Traveling-Wave Tube

H. D. ARNETT, H. E. BROWN, J. T. JENSEN, JR., R. H. KYSER,
S. T. SMITH, N. R. VANDERPLAATS, AND L. M. WINSLOW

*Electronics Technology Division*

July 31, 1975

**NAVAL RESEARCH LABORATORY**
**Washington, D.C.**

SECURITY CLASSIFICATION OF THIS PAGE *(When Data Entered)*

| REPORT DOCUMENTATION PAGE | | READ INSTRUCTIONS BEFORE COMPLETING FORM |
|---|---|---|
| 1. REPORT NUMBER<br>NRL Report 7899 | 2. GOVT ACCESSION NO. | 3. RECIPIENT'S CATALOG NUMBER |
| 4. TITLE *(and Subtitle)*<br>THE NRL FLUID-COOLED HELIX TRAVELING-WAVE TUBE | | 5. TYPE OF REPORT & PERIOD COVERED<br>Final report on one phase of a continuing NRL problem.<br>6. PERFORMING ORG. REPORT NUMBER |
| 7. AUTHOR(s)<br>H. D. Arnett, H. E. Brown, J. T. Jensen, Jr., R. H. Kyser, S. T. Smith, N. R. Vanderplaats, L. M. Winslow | | 8. CONTRACT OR GRANT NUMBER(s) |
| 9. PERFORMING ORGANIZATION NAME AND ADDRESS<br>Electronics Technology Division<br>Naval Research Laboratory<br>Washington, D.C. 20375 | | 10. PROGRAM ELEMENT, PROJECT, TASK AREA & WORK UNIT NUMBERS<br>NRL Problem R06-45<br>Project XF-54-545-014 |
| 11. CONTROLLING OFFICE NAME AND ADDRESS | | 12. REPORT DATE<br>July 31, 1975<br>13. NUMBER OF PAGES<br>58 |
| 14. MONITORING AGENCY NAME & ADDRESS*(if different from Controlling Office)*<br>Department of the Navy<br>Naval Electronics Systems Command<br>Washington, D.C. 20360 | | 15. SECURITY CLASS. *(of this report)*<br>Unclassified<br>15a. DECLASSIFICATION/DOWNGRADING SCHEDULE |

16. DISTRIBUTION STATEMENT *(of this Report)*

Approved for public release; distribution unlimited.

17. DISTRIBUTION STATEMENT *(of the abstract entered in Block 20, if different from Report)*

18. SUPPLEMENTARY NOTES

19. KEY WORDS *(Continue on reverse side if necessary and identify by block number)*

Fluid cooling, helix, High power, Microwave amplification, Traveling-wave tubes

20. ABSTRACT *(Continue on reverse side if necessary and identify by block number)*

In the conventional helix traveling wave tube the helix is supported by three or four ceramic rods between the helix and tube shell. The amount of average power attainable is limited by the amount of heat that can be conducted along the helix and across the ceramic supports. A fluid-cooled helix was designated that employs a helix made of copper tubing supported by hollow ceramic tubing brazed at each half turn of the helix. Several geometries of fluid flow and their effect on the RF design of the tube were tested. The cooling analyses indicate that it should be possible to dissipate at least five times as much power with the fluid cooling as with conventional

DD FORM 1 JAN 73 1473 EDITION OF 1 NOV 65 IS OBSOLETE
S/N 0102-014-6601 |



SECURITY CLASSIFICATION OF THIS PAGE *(When Data Entered)*

20. Continued

thermal conduction for frequencies up through S-band. For some fluids the circuit RF losses increase rapidly with frequency above the operating frequency. This is useful for suppressing unwanted backward-wave oscillations. Experimental tubes were built and tested. Four kilowatts of average power was attained at 3 GHz in a design that was capable of octave bandwidth operation.

CONTENTS

# THE NRL FLUID-COOLED HELIX TRAVELING-WAVE TUBE

## INTRODUCTION

In a traveling-wave tube (TWT) amplifier, a well-focused electron beam passes through, or in proximity to, a slow-wave circuit and then to a collector. At the input end of the circuit a radio-frequency (RF) signal is injected, and the electron beam interacting with the electromagnetic fields of the circuit gives up some of its energy to the circuit. In this way high-gain amplification of the signal over a range of frequencies is produced.

The unifilar helix is the most commonly used TWT circuit. This is because it has the widest bandwidth of any slow-wave circuit, while at the same time it produces a desirable high interaction impedance to the electron beam. A disadvantage of the helix circuit is the difficulty in removing waste heat produced by both RF ohmic losses and by electron-beam interception at the helix.

In the conventional design, the helix is supported by three or four ceramic rods between the helix and tube shell, or barrel, as shown in Fig. 1a. The heat is removed by thermal conduction from the helix through these rods, which may be beryllia, alumina, or boron nitride. Lucken [1, 2] has discussed the power dissipation limitation of dielectric support rods of this type. In general, heat removal is improved by good thermal contacts at the ceramic-to-helix and ceramic-to-barrel interfaces. If too much ceramic is used, however, the increased dielectric loading limits the bandwidth and lowers the interaction impedance and efficiency.

A more effective method of heat removal that introduces a minimum of dielectric loading is needed. In the early days of TWT development (1948-1958) there were some partly successful attempts [3-5] to cool the helix by making the helix out of metal tubing and pumping a coolant through this tubing from one end to the other. To obtain sufficient flow for adequate cooling by this method, fluid pressures greater than 1,000 psi were required. This is too high to be practical. In the method to be described here, the fluid can be introduced and/or extracted at each half turn of the helix. This reduces the required pressure to 50 psi or less, while at the same time providing low dielectric loading, maintaining high interaction impedance, and suppressing backward-wave oscillations.

The fluid-cooled helix described in this report employs a helix made of copper tubing and supported by hollow ceramic tubing brazed to each half turn of the helix. The coolant may enter the ceramic tubing on one side of the helix, flow through the helix, and then flow out through the ceramic tubing on the other side of the helix as shown in Fig. 1b. Various flow configurations, fluids, flow rates, RF losses, and other limiting factors are discussed in determining the optimum balance between helix cooling and satisfactory electrical performance.

Note: Manuscript submitted April 15, 1975.

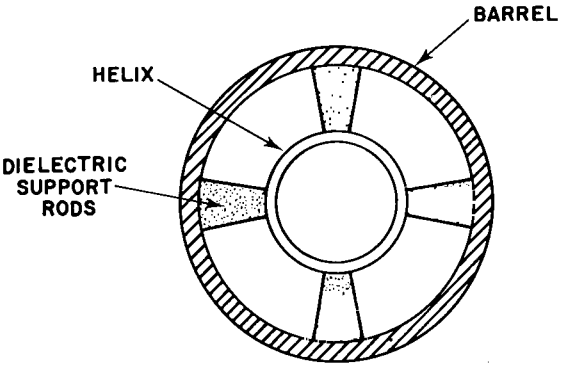


(a)

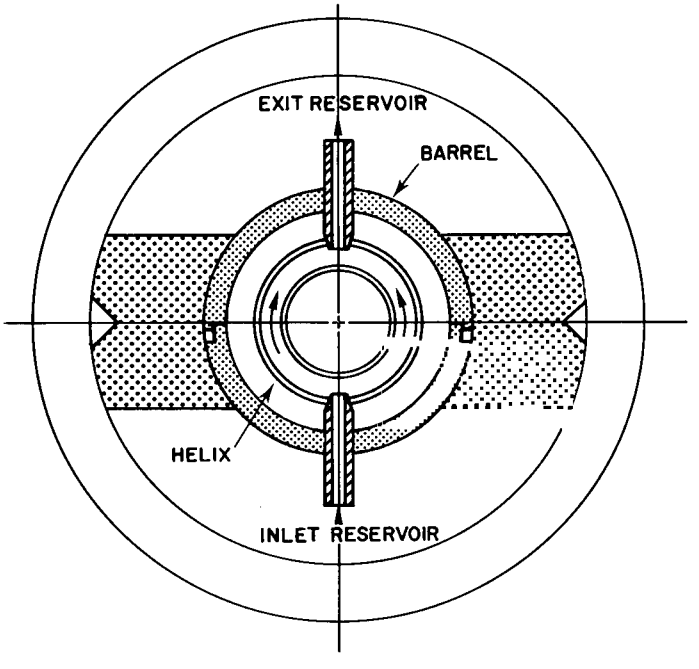


(b)

Fig. 1 — Cross-sectional views of helix traveling wave tubes
(a) Conventional rod-supported helix (b) Fluid-cooled helix

A very useful byproduct of fluid cooling is that the RF loss increases rapidly with frequency above the operating band of the TWT with some fluids. This frequency-selective loss has been utilized to suppress the backward-wave oscillations that usually limit the peak power that can be attained in helix traveling-wave tubes. Experimental data are presented for a design that has produced 4 kW of CW power and 11.1 kW of pulse power at 3000 MHz.

## FLUID FLOW METHODS

As shown in Fig. 1b, ceramic tubes are brazed to each half turn of the helix tubing and to the copper barrel. These ceramic tubes act not only as mechanical supports for the helix but also as a means of introducing and extracting the cooling fluid. Two methods of brazing the ceramic tubes to the helix and barrel have been developed at the Naval Research Laboratory. These methods are described in detail in Appendix A. Three flow geometries used are crossed, axial, and hybrid flow.

In what has been called crossed flow, the fluid flows from the inlet reservoir on one side of the tube envelope, into the ceramic tubes, then through half turns of the helix, and finally out the ceramic tubes on the opposite side of the helix to the exit reservoir. The output lead, which is to become the center conductor of a coaxial line, either becomes a solid copper wire or there is a blockage at the output, as shown in Fig. 2a. Crossed flow provides the highest total fluid flow through each section of the helix. However, it does not provide as much cooling in the last few turns of the helix as provided by other methods to be described, and it gives no cooling at all in the coaxial output lead where the RF power and heat are the highest.

When axial flow is employed, the helix is supported in exactly the same fashion as described above, but the copper tubing is continued through the output window and output coaxial line. Fluid is forced into the helix tubing through all the ceramic tubes, as shown in Fig. 2b; the direction of fluid flow may be reversed equally well, with the coolant flowing in from the output and out through the ceramic support tubes. Axial flow provides maximum cooling of the output lead, since all of the fluid flows through the last part of the helix and the inner conductor of the output line. The fluid flow decreases in succeeding half turns of the helix away from the output.

If the helix tubing is allowed to remain open in the output, as is the case in axial flow, and fluid is pumped across the helix as in cross flow, then there is considerable flow of coolant in the output conductor. The result is axial flow in the last few turns of the helix and cross flow at a distance away from the output. This type of flow, called hybrid flow, is illustrated in Fig. 2c. Hybrid flow can yield the largest total flow of fluid for a given pressure drop. One feature of hybrid flow is that in the helix half turn where the flow changes from axial flow to cross flow there is no flow at all. This can be a disadvantage to hybrid flow, if this transition point is too near the output.

There are some additional variations on the flow illustrated by Figs. 2a, b, c. In the case of axial and hybrid flow, the ceramic tubing supports may be omitted on the last few turns, for example. In the case of hybrid flow, obstructions may be placed in the outlet ceramics. This causes the helix half turn without flow to move farther from the output end of the tube.

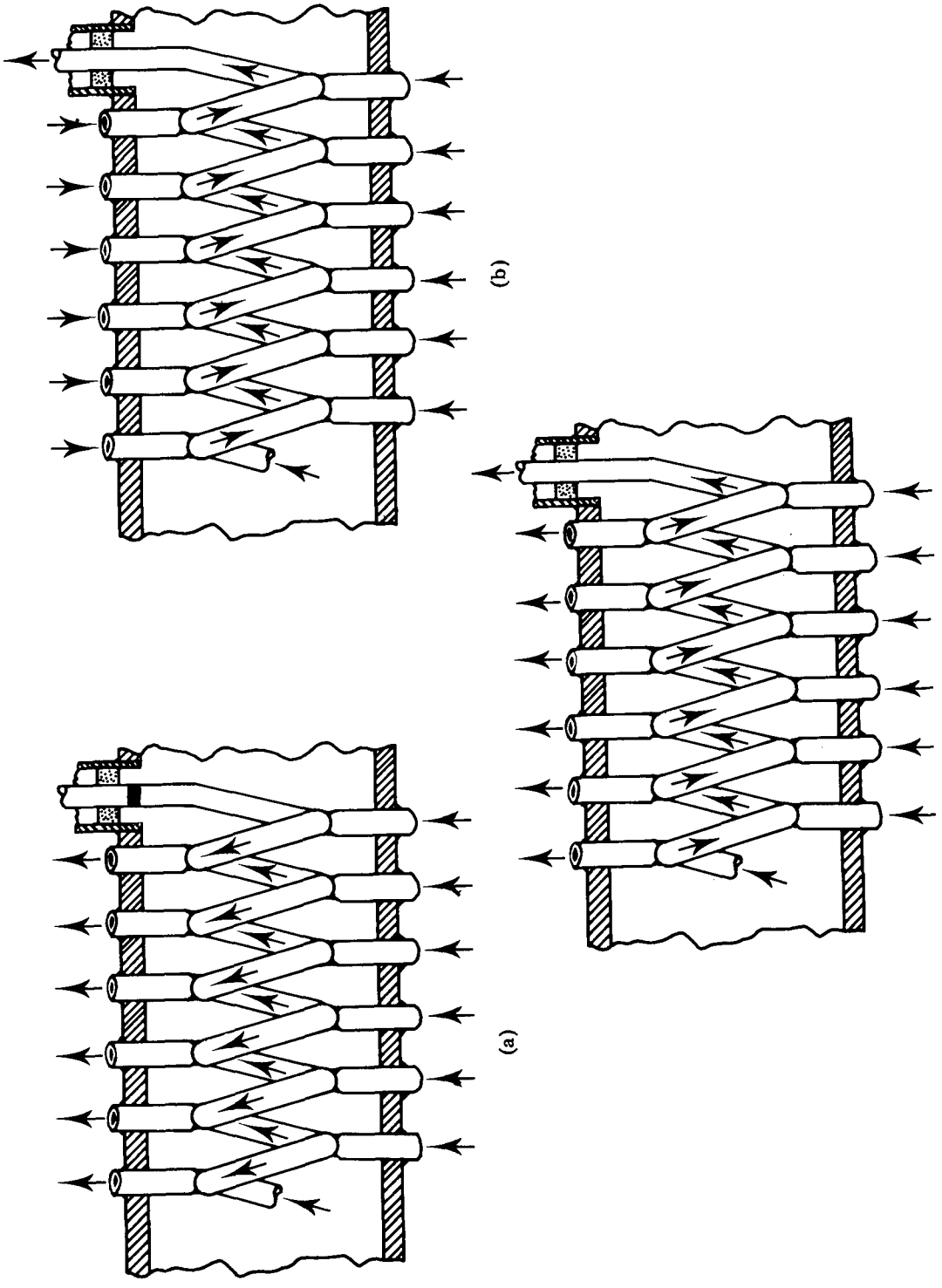


Fig. 2 — Fluid-flow geometries for fluid-cooled helix traveling wave tubes (a) Cross flow (b) Axial flow (c) Hybrid flow

In a complete traveling-wave tube different types of flow may be used in different sections of the tube. For example, axial or hybrid flow may be used in the output section and cross flow in the attenuator section.

## HELIX COOLING

The major concern, of course, in cooling the helix is in maintaining the outside temperature of the helix tubing to within a tolerable limit while it is being heated by electron-beam interception and by RF power losses. In going from the inlet temperature reservoir where the temperature is $T_i$ to the surface of the helix tubing where the temperature is $T$, several temperature increments can be identified. First, as the fluid flows through the inlet ceramic it absorbs some RF power and experiences a temperature change $\Delta T_c$. As the coolant passes through a helix half turn, it absorbs all the RF and electron-beam interception power on that half turn and experiences a further temperature change $\Delta T_h$. At the interface between the moving fluid and the surface of the tubing there is a thin quiescent layer of fluid. Heat flows across this thin layer by thermal conduction, and since the conductivity of fluids is quite low a temperature increment $\Delta T_D$ of some size can occur here. Heat also flows by conduction through the thin wall of the tubing from the outer surface to the inner surface. The temperature increment associated with this is considered to be negligible. The case that has been considered here and for which the equation

$$T = T_i + \Delta T_c + \Delta T_h + \Delta T_D \tag{1}$$

can be written is that for cross flow. The more involved cases of axial flow and hybrid flow, together with some aspects of the fluid flow in cross flow, are discussed in detail in Appendixes B and C.

The two temperature increments $\Delta T_c$ and $\Delta T_h$, which arise from the absorption of heat into the fluid, are readily calculated from the basic definition of heat capacity. They are given by

$$\frac{\Delta T}{P_t} = \frac{3.79 \times 10^{-3}}{cgF} . \tag{2}$$

The numerical factor in Eq. (2) is the proper one to use if $\Delta T$ is the temperature increment in degrees $C$, $P_t$ is the power input to the fluid in watts, $c$ is the specific heat of the fluid in Btu/lb °F, $g$ is the specific gravity of the fluid relative to water, and $F$ is flow rate of the fluid in gallons per minute. If $P_t$ is the heat flow through the helix wall, Eq. (2) gives the temperature rise $\Delta T_h$ of the coolant flowing through the half turn of helix; if $P_t$ is the heat absorbed by the fluid in flowing through the ceramic tube, Eq. (2) gives the temperature rise $\Delta T_c$. The RF power absorbed in the fluid in passing through the ceramic tubing, in addition to affecting the temperature rise of the helix, has a bearing on the RF design of the traveling-wave tube. This factor is discussed later in considering the attenuator design.

The quantity of fluid flow for a given pressure and the amount of cooling for a given flow depends, among other things, on whether the flow is turbulent or laminar.

Turbulent flow causes more fluid mixing and therefore ensures more effective heat exchange from the inner walls of the tubing to the cooling fluid. Turbulent flow is indicated by high values of Reynolds numbers, with the transition from laminar to turbulent flow beginning at Reynolds numbers approximately between 1500 and 2300. For the units used throughout this report, the Reynolds number is given by

$$R_D = 7650 \frac{Fg}{D\mu} , \tag{3}$$

where $D$ is the equivalent diameter of the tubing and $\mu$ is the absolute viscosity of the fluid in lb/hr ft. The quantities $F$ and $g$ have been defined in discussing Eq. (2). This gives the transition flow rate between laminar and turbulent flow as

$$F_T = 0.20 \frac{D\mu}{g} , \tag{4a}$$

if the transition value of the Reynolds number is 1500; and

$$F_T = 0.30 \frac{D\mu}{g} , \tag{4b}$$

if the transition value of the Reynolds number is 2300.

The amount of cooling for a given geometry depends on the flow rate, which in turn depends on the available fluid pressure. Figures 3a and 3b show experimentally measured pressure drops at different flow rates for cross, hybrid, and axial flow. For the measurements of Fig. 3a the fluid was water, whereas for Fig. 3b it was FC-43. The experiments were performed with a 6-turn section of helix having 11 ceramic tubes. The helix was wound to a mean diameter of 0.307 in., with 6 turns per inch. Thus the distance along the helix between ceramics was 0.489 in. The outer diameter of the helix tubing was 0.060 in. in all cases.

In the case of cross flow, the plotted flow rate is the average flow rate in the helix. The average flow rate through the ceramics is twice that in the helix. The three curves on the right-hand side of Figs. 3a and 3b are for hybrid and axial flow, and the plotted flow rate is the flow rate through the open end of the helix. These measured flow rates are in reasonable agreement with the theory presented in Appendix C.

Cooling rates for these flow rates can be calculated from the equations of Appendix B, which give the temperature rise from heat absorbed into the fluid and the duct temperature rise between the bulk of the fluid and the helix wall under various flow conditions. By far the largest temperature rise is that in the duct between the fluid and helix wall. Cooling rates for the S-band helix geometry are shown in Fig. 4 for various fluids. As expected, the cooling is quite dependent on the flow rate and the nature of the flow (turbulent or laminar). If cooling ability alone is considered, water is by far the optimum fluid, but it has RF losses that limit the size of the ceramic tubing that can be used with it.

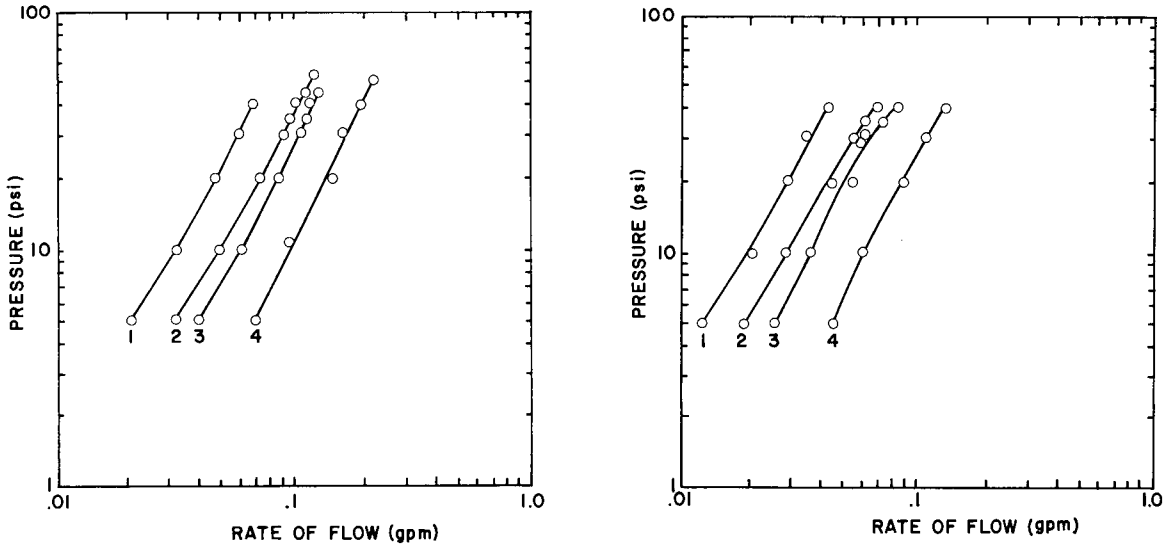


(a) Measurements made using a 6-turn helix and 11 ceramics with water as a coolant
1—Average cross flow per half turn using 0.050-in. I.D. tubing and 0.032-in. I.D. ceramics
2—Hybrid flow out the end of helix using 0.040-in. I.D. tubing and 0.020-in. I.D. ceramics
3—Hybrid flow out the end of helix using 0.050-in. I.D. tubing and 0.032-in. I.D. ceramics
4—Axial flow using 0.050-in. I.D. tubing and 0.032-in. I.D. ceramics

(b) Measurements made using a 6-turn helix and 11 ceramics with FC-43 as a coolant
1—Average cross flow per half turn using 0.050-in. I.D. tubing and 0.032-in. I.D. ceramics
2—Hybrid flow out the end of helix using 0.040-in. I.D. tubing and 0.020-in. I.D. ceramics
3—Hybrid flow out the end of helix using 0.050-in. I.D. tubing and 0.032-in. I.D. ceramics
4—Axial flow using 0.050-in. I.D. tubing and 0.032-in. I.D. ceramics

Fig. 3 — Measured flow rates for an S-band fluid-cooled helix. The average helix diameter was 0.307 in. and there were 6 turns per inch.

Also shown in Fig. 4 are calculated cooling rates for a conduction-cooled helix supported by four BeO or BN rods under conditions favorable for maximum cooling. When fluid-cooled helices operated under conditions of cross flow are compared with the conduction-cooled helices, the conduction-cooled helices are comparable or perhaps superior. But when fluid-cooled helices under axial flow conditions are considered, the fluid-cooled helix offers a higher cooling rate at S-band by as much as an order of magnitude.

## CIRCUIT DESIGN OF THE TUBE

The circuit parameters needed in the design of the fluid-cooled helix TWT are the phase velocity, the interaction impedance, and the RF attenuation as functions of frequency and axial position. From these and the electron beam parameters the overall performance of the tube can be predicted.

The phase velocity is shown in Fig. 5 for the geometry indicated there. Shown are theoretical curves [6] of phase velocity vs frequency for the sheath helix model in free space, the sheath helix model within a shield, the real helix with finite wire size but without dielectric loading, and then finally the real helix with ceramic tubing supports.

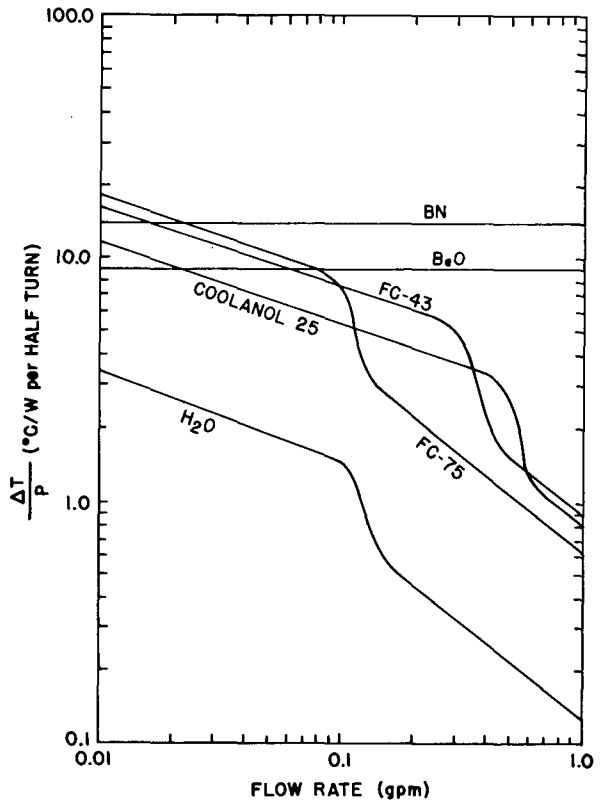


Fig. 4 — Computed temperature rise of coolant as a function of flow rate for several coolants for the S-band helix. To the left of the breaks the flow is laminar, while to the right it is turbulent. Also shown for comparison are the cases of a 4-rod supported helix with either beryllia or boron nitride as the rod material.

For the last two curves there is also shown experimental confirmation of the computations. For the dielectric-supported helix, alumina tubing was used. The fraction by which the phase velocity is reduced by the dielectric support is called the dielectric loading factor (DLF). In this case the dielectric loading factor has the high value of 0.9, compared to the typical value of about 0.8 for conventional rod-supported helices. This high dielectric loading factor means that the dielectric has minimal loading effects, and this aids in producing a high interaction impedance for the circuit. The impedance [6] of the present fluid-cooled circuit is shown as a function of frequency in Fig. 6.

The choice of 0.060 in. as the outer diameter of the helix tubing (0.050 in. I.D.) was based initially on availability. This is probably not the optimum size for an S-band fluid-cooled helix TWT. For some types of cooling geometry, the fluid flow can be increased by using larger diameter helix tubing, but this may adversely affect the RF performance of the tube.

In the case of cross-flow geometry most of the pressure drop occurs at the points of constriction where the fluid enters the entrance and exit ceramics. In the cases of axial and hybrid flow, however, a larger helix tubing diameter, in general, increases the flow of

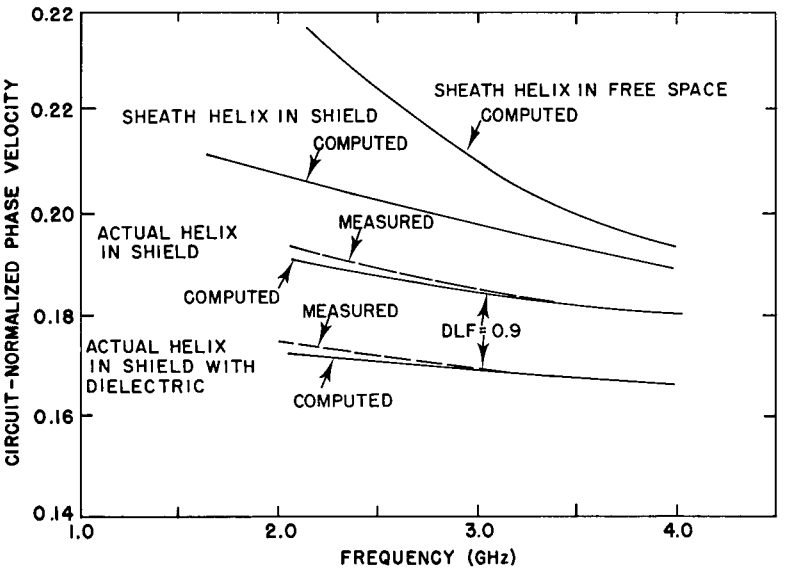


Fig. 5 — Phase velocity for various configurations, with helix mean diameter 0.307 in., wire diameter 0.060 in., pitch 0.167 in., and shield diameter 0.507 in.

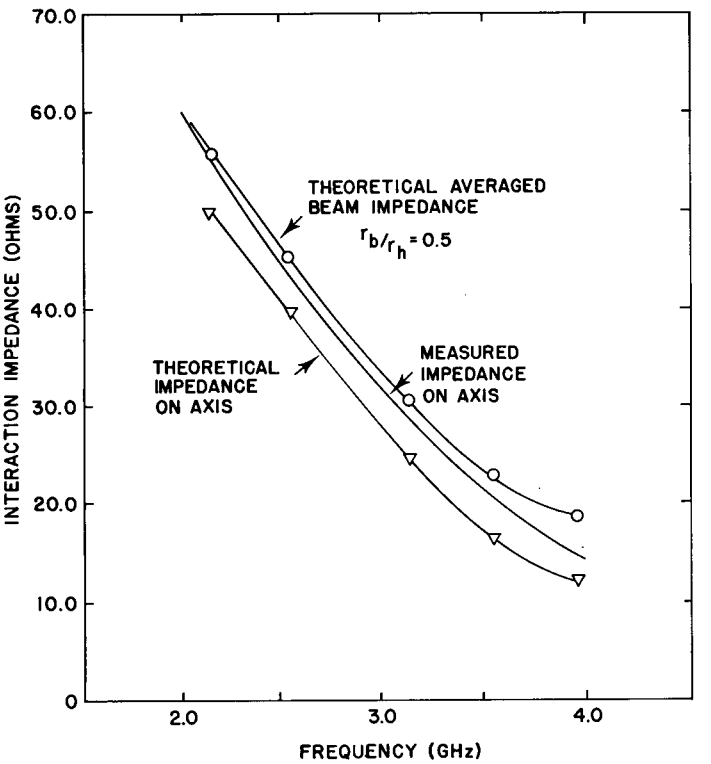


Fig. 6 — Computed and measured helix interaction impedances as a function of frequency for a helix of the same dimensions as in Fig. 5

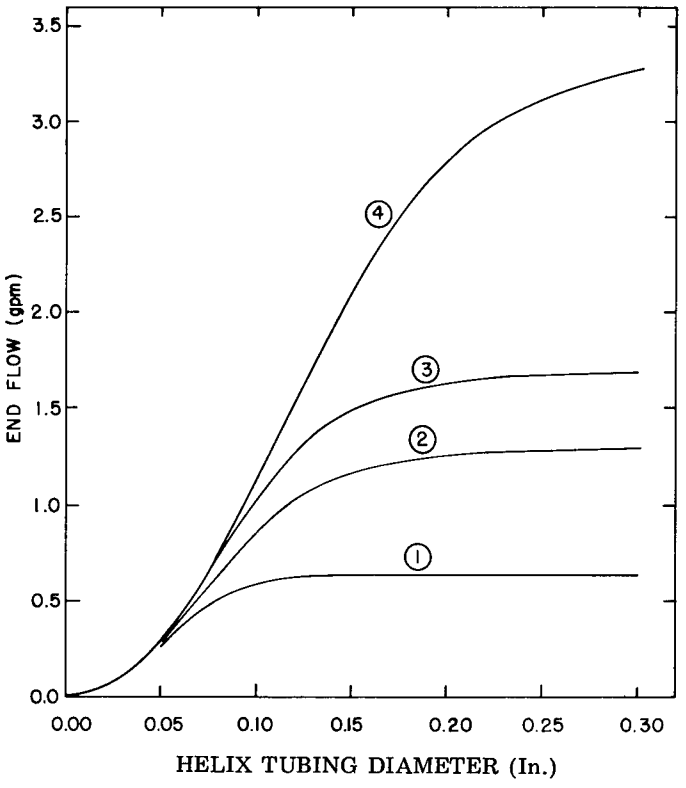


Fig. 7 — Computed water flow rate as a function of helix tubing diameter for axial flow. ① Five-turn helix and 0.020-in. I.D. ceramics, ② Ten-turn helix and 0.020-in. I.D. ceramics, ③ Five-turn helix and 0.030-in. I.D. ceramics; ④ Ten-turn helix and 0.030-in. I.D. ceramics. (Assumed pressure drop = 50 psi.)

coolant. Shown in Fig. 7 are some predictions of coolant flow rates, based on material in Appendix C, for the case of axial flow with water as the coolant. For small helix tubing sizes and for the two ceramic diameters considered, the flow out the end of the helix depends almost entirely on the size of the helix tubing; it is nearly independent of the ceramic diameter and the number of ceramics involved in the flow. As the helix tubing size is increased, the flow is limited by the ceramic size and the number of ceramics. With very large helix tubing diameter, nearly all of the pressure drop occurs in the ceramics, and the flow is just the limiting flow for one ceramic multiplied by the number of ceramics. In the case of hybrid flow, the limiting flow out the end of the helix would be about one-half that predicted for axial flow.

For axial flow, the manner in which the total flow is distributed among the individual sections of helix is determined by the ceramic diameter. The predictions for 0.050-in.-diameter helix tubing and a 10-turn helix are shown in Fig. 8. The use of 0.030-in.-diameter ceramics gives the largest total fluid flow, but the flow decreases quite rapidly away from the output. For the case of 0.011-in.-diameter ceramics, the flow is beginning to be limited by the ceramic size; the total flow is not greatly different than that for the 0.032-in. ceramics, and the flow in individual sections of the helix decreases almost linearly away from the output.

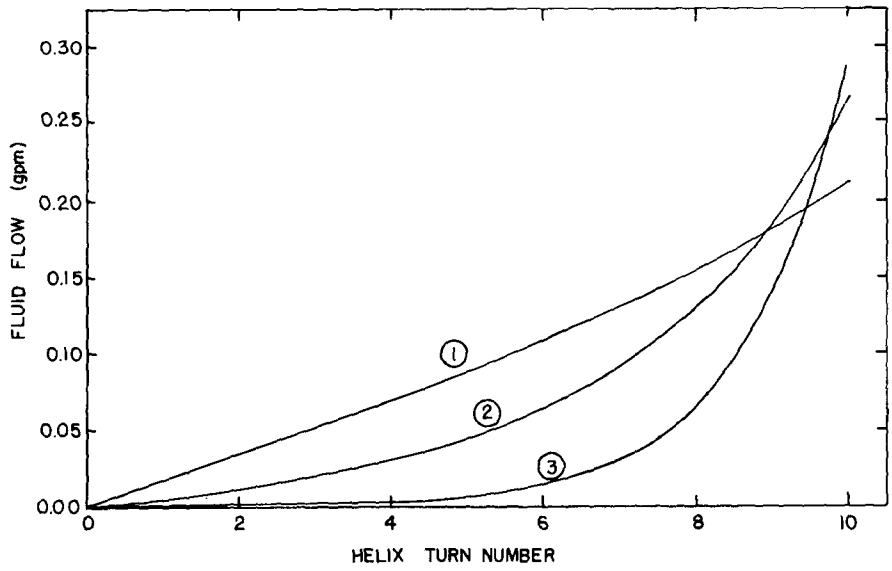


Fig. 8 — Computed distribution of water flow as a function of helix turn number for a helix with axial flow. The helix tubing inner diameter is 0.050-in. and the ceramic inner diameter is the parameter. ① Ceramic inner diameter is 0.011 in.; ② Ceramic is 0.020 in.; ③ Ceramic inner diameter is 0.032 in.

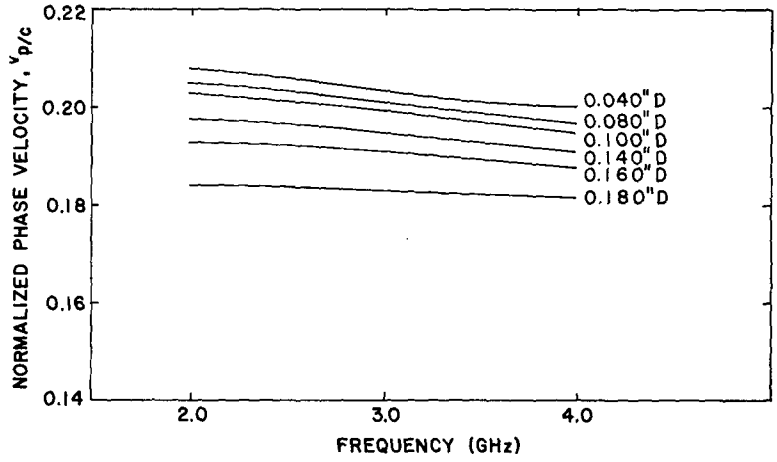


Fig. 9 — Computed helix phase velocity as a function of frequency for different helix wire diameters for a helix with 5 turns per inch; barrel diameter 0.507 in.; helix diameter 0.307

For a TWT helix having 6 turns per inch, as was the case here, the outer diameter of the helix cannot exceed 1/6 in., or adjacent turns will be touching. Long before this limit has been reached the RF performance of the helix will have deteriorated. Figure 9 shows the variation of phase velocity, and Fig. 10 shows the variation of interaction impedance as the helix wire diameter is changed for a helix with 5 turns per inch. More damaging than the reduced interaction impedance is the fact that as the helix tubing size is increased there is less space available for the electron beam. The smaller beam diameter results in the requirement for a higher magnetic focusing field and also increases the space-charge density in the beam. This means a heavier tube, and, if the space-charge density becomes

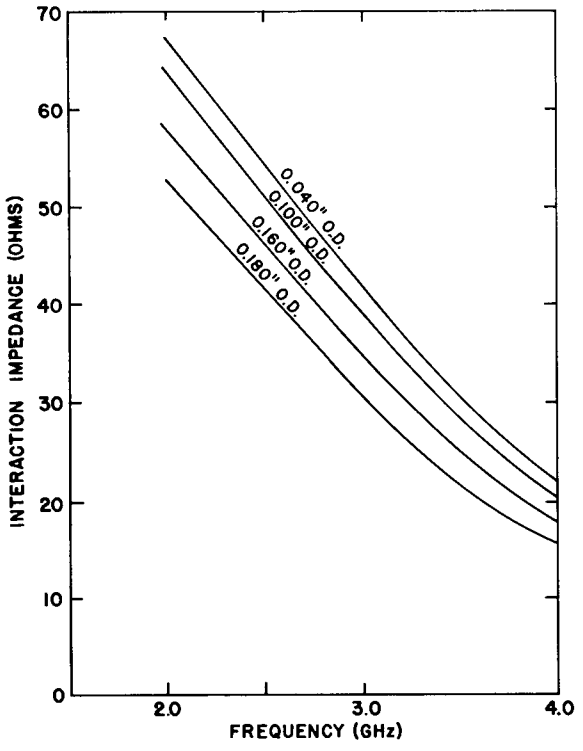


Fig. 10 — Computed helix interaction impedance on the axis as a function of frequency for different helix wire diameters, for a helix of the same dimensions as in Fig. 9

too high, a decrease in efficiency at the low end of the frequency band. It is probably true, however, that some increase in helix tubing size would lead to an overall improvement in tube performance.

As the RF signal moves down the helix, high RF fields are established between the helix and the barrel. In addition to the usual skin-effect RF losses of the helix, the presence of the coolant within the ceramic tubes adds additional shunt losses between the helix and the barrel. Radio-frequency loss has both good and bad effects on tube operation. Hence, this is an important part of the tube design.

The RF loss as a function of frequency for different fluids is shown in Fig. 11. Here the loss has been plotted in terms of Pierce's normalized loss parameter $d$. The rapid rise in loss at the higher frequencies (above the useful bandwidth of the TWT) is due in part to the resonant rise in RF impedance near the upper band edge of the helix filter circuit. This frequency selectivity of the loss is an advantageous byproduct in that it can be used to suppress the unwanted backward-wave oscillations that usually limit the amount of peak power that can be attained in helix TWTs. In this tube the backward-wave oscillation frequency is about 6.2 GHz, where Fig. 11 shows the loss to be quite high. It can be shown that the basic criterion for the prevention of oscillations is that the normalized value of the backward-wave parameter $d_{-1}$ must be greater than a value of 1.5 at the backward-wave frequency.

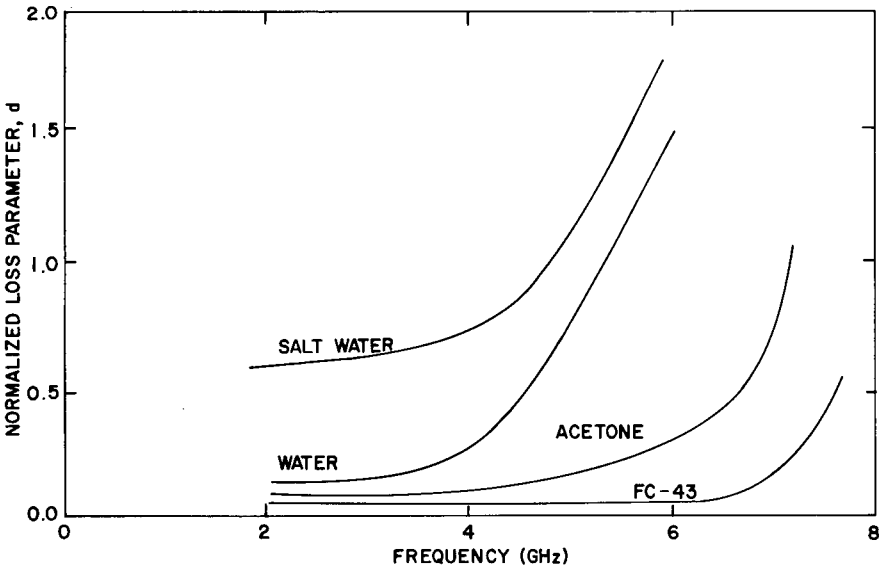


Fig. 11 — The Pierce normalized loss parameter $d$ as a function of frequency for 0.032 inch I.D. support ceramics. This illustrates the frequency selectivity of the fluid-cooled helix RF loss.

The presence of the coolant within the ceramic support adds significant loss in the useful frequency passband of the TWT, as shown in Fig. 12. The shunt loss is least with the ceramics alone, slightly higher with the low-loss coolant FC-43 within the ceramic, and significantly higher when water is used as the coolant. A method of reducing the RF losses for water is to reduce the inner diameter of the ceramic tubes from 0.032 to 0.020 in., as shown in Fig. 12. This reduces the cross-sectional area of the water flow and therefore reduces the RF loss. Unfortunately, however, a reduction in fluid flow accompanies any decrease in ceramic diameter. In the case of cross-flow geometry the flow rate is almost totally dependent on the ceramic cross section; the fluid flow rate varies at least as the square of the inner diameter of the ceramics (see Appendix C). If either axial or hybrid flow is used to cool the helix, fluid flows in parallel through several ceramic channels, and the flow at the output end of the helix is much less affected by the diameter of the ceramic supports.

The prime effect of the RF loss in the operating band is to decrease the TWT efficiency. This efficiency loss is illustrated in Table 1 for each coolant and ceramic size. Traveling-wave tube parameters of $C = 0.1$ and $b = 1.5$ are assumed. The calculations of Table 1 are based on the loss data for 3 GHz. The electronic efficiency is calculated by Eq. (5) of Ref. 6.

It can be seen from Table 1 that the RF losses have an appreciable effect on the efficiency. This efficiency reduction can be minimized by using FC-43 as the coolant or by using axial or hybrid flow without any flow injected into the ceramic tubes of the last few turns at the output where the RF power is highest, or both. Incidentally, the actual efficiency can be increased above the electronic efficiency by well-known collector depression techniques.

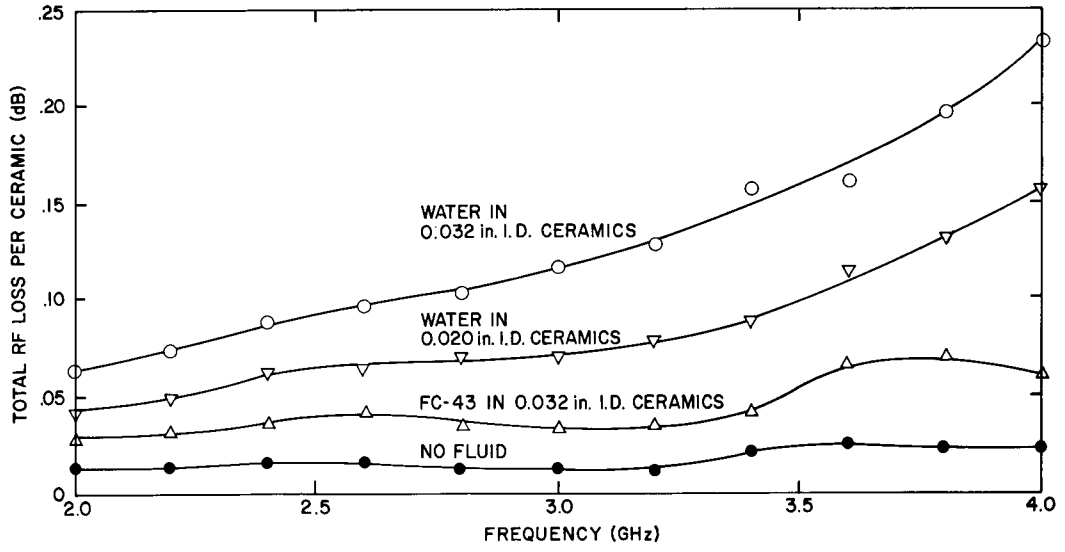


Fig. 12 — Helix RF loss per ceramic as a function of frequency for different ceramic sizes and coolants

Table 1

| Coolant | Ceramic Size (I.D., in.) | Loss per Ceramic (dB) | Loss Parameter | Electronic Efficiency |
|---|---|---|---|---|
| Water | 0.032 | 0.117 | 0.171 | 0.15 |
| Water | 0.020 | 0.070 | 0.103 | 0.22 |
| FC-43 | 0.032 | 0.033 | 0.048 | 0.30* |
| None | 0.032 | 0.013 | 0.019 | 0.35* |

*The tube may oscillate under these conditions.

All high-gain traveling-wave tubes require an attenuator to keep the output reflected power from reaching the input and thus causing regenerative oscillations. In this tube the RF loss depends on the conductivity of the coolant as well as on the cross-sectional area of the fluid flowing in the ceramic tubes. The attenuator is a distributed-loss attenuator, in which the normalized loss parameter $d$ can be varied between a value of 0.05 and about 3 by varying the conductivity of the fluid used. In this tube a ceramic tubing of 0.032 in. I.D. was chosen to increase the cross-sectional area and thereby the electrical conductance of the cooling fluid that flows through the ceramics in the attenuator region. A further increase in conductivity was achieved through the use of salt water in controlled concentrations. The RF loss as a function of the mole concentration of sodium chloride in water is given in Fig. 13. As can be seen from the three curves of Fig. 13,

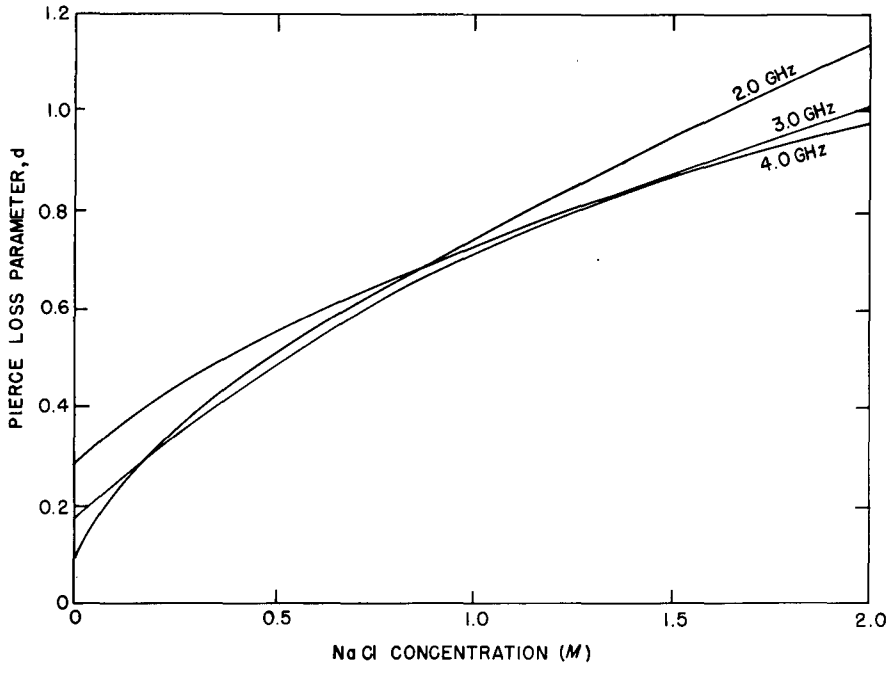


Fig. 13 — Pierce loss parameter $d$ as a function of sodium chloride concentration for the distributed-loss attenuator

the RF loss is relatively independent of frequency within the operating band of 2 to 4 GHz.

Most attenuators in traveling-wave tubes are located in the vacuum. In the fluid-cooled attenuator the power is absorbed in a fluid moving outside the vacuum. Because no gas is generated within the vacuum, large amounts of power can be absorbed in the attenuator.

The power-handling capability of the fluid-cooled attenuator depends on both the loss per turn and the fluid flow rate per turn. In the design now employed at the Naval Research Laboratory, it is estimated that the attenuator can absorb 7 kw of RF power. This means that the present tube can operate into a short circuit without damage to the internal attenuator.

An alternate method to that of using conducting salt water might be to place a lossy member inside the coolant support channels in the region of the attenuator. These elements could then be cooled by a low-loss fluid. This would allow operation with only one type of coolant.

## EXPERIMENTAL RESULTS

The Naval Research Laboratory has constructed and tested 6 medium-gain traveling-wave tubes with fluid-cooled helices. All were designed for operation in the 2- to 4-GHz region. A typical helix was 7 in. long and was made of thin-walled copper tubing having an outer diameter of 0.060 in. The inside diameter of the helix was 0.247 in., and

there were 6 turns per inch. The number of ceramic support tubes was 82, thus requiring 164 metal-to-ceramic brazes. The barrel diameter was 0.507 in. in some tubes and 0.625 in. in others. The tubes used an electron gun having a perveance of $2.1 \times 10^{-6}$ $(A/V^{3/2})$ which produces an electron beam with nominal beam diameter of 0.170 in. The spent beam impinged on a single-stage water-cooled copper collector.

The helix was comprised of three sections. There was an input section 1 in. long followed by an attenuator 2 in. long and finally an output section 4 in. long. Thin-walled alumina ceramic supports (0.032 in. I.D. 0.065-in. O.D.) were used in the attenuator section along with salt water as the high-loss fluid. Heavy-walled alumina ceramic supports (0.020-in. I.D., 0.065-in. O.D.) were used in the input and output sections with water as the cooling fluid to provide frequency-selective loss for suppressing backward-wave oscillations.

Hybrid flow was used in cooling the output section. The fluid-cooled output lead passed through a ceramic coaxial output window and then into a ridged waveguide, from which the RF power was extracted. The water exhaust of the output lead occurred after the lead passed through the ridged waveguide.

The attenuator section of the tube used cross-flow cooling and separate input and output manifolds. A controlled amount of salt was added to the coolant until it had sufficient attenuation to isolate the input signals from the output and thus avoid regenerative oscillations. Because the attenuator was distributed, it also aided in suppressing backward-wave oscillations.

Figure 14 shows the output vs input characteristics of one of the tubes under pulse operation with water cooling. The frequency was 3 GHz, and the peak power of about 8.6 kW was observed with an electronic efficiency of 27% without collector depression when the tube was operated at 12 kV. The efficiency could be increased to about 40% with collector depression. Because of the distributed attenuator, the input-output characteristic had an extended range with little degradation of power beyond saturation. If the losses had not increased with frequency as shown in Fig. 11, backward-wave oscillations would have been observed before the conditions for obtaining 8.6 kW output power could have been reached. Figure 15 shows the measured pulse output power of the same tube over the S-band frequency range at two different voltages for a drive power of 100 W. This RF drive level was insufficient to saturate the tube over most of the frequency band.

One of the later tubes produced 4 kW of average power for approximately 5 min. During the time that the average power was 4 kW, the measured temperature rise of the water from the output lead was less than 15°C. Hybrid flow was used in the output section with water as the coolant through 0.020-in. I.D. ceramic supports.

The results described above were obtained from the first and third medium-gain TWTs tested. The original measurements indicated that an RF power of 12 kW had been achieved at 3 GHz with an electronic efficiency of 37% and over 50% efficiency with collector depression. A careful check of the calibration of the RF test equipment, which indicated the possibility of significant errors in the original measurements, was made some months later, using newly available calibration equipment. Whether the original calibration was significantly in error cannot be determined. However, the data reported here were corrected to reflect the latest calibration, which gives the most conservative power measurement.

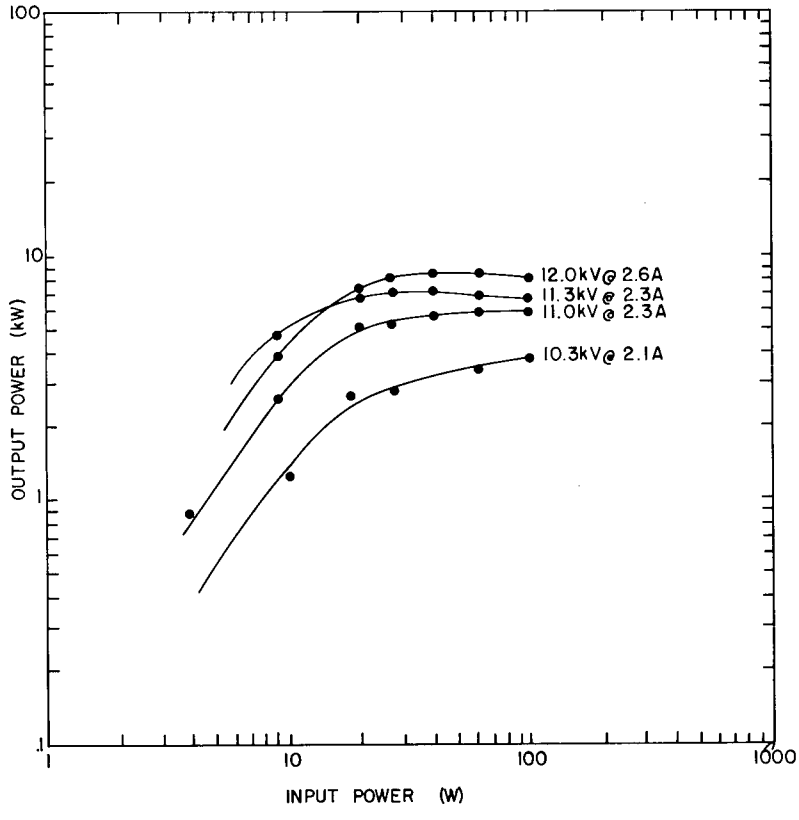


Fig. 14 — Input-output performance characteristics for tube 1. Frequency is 3 GHz.

The following describes the performance and final failure modes of the 6 tubes that were built.

The first and second tubes suffered from vacuum leaks in the coaxial windows that prevented normal high-temperature bakeout. The data shown in Figs. 14 and 15 were taken on the first tube, which yielded up to 8.6 kW peak power at 3.0 GHz and 12 kV beam voltage. The electronic efficiency was 27% under pulsed conditions, and this could be increased to over 40% by collector depression. The second tube yielded about 5.8 kW peak power at a beam voltage of 11 kV. These first two tubes failed under test due to cathode deactivation caused by vacuum leaks at the RF output window. The brazing technique used initially was inadequate to keep the thermal stresses during tube assembly and testing from causing vacuum leaks in the RF window metal-ceramic seals.

The third tube was processed with a good vacuum and yielded the highest average power. During RF testing at 4 kW average power, an AC breaker which supplied the solenoid power failed due to an overload. This failure allowed the electron beam-focusing field to fall slowly, over a time of several seconds. This rate of decrease prevented activation of the protective circuitry in time to prevent helix burnout. The result was catastrophic failure of the helix after about 5 min of operation at the 4-kW power level.

The fourth tube failed because of an RF arc in the choke of the output window while it was being operated at about 9 kW peak power and 20% duty. This tube had

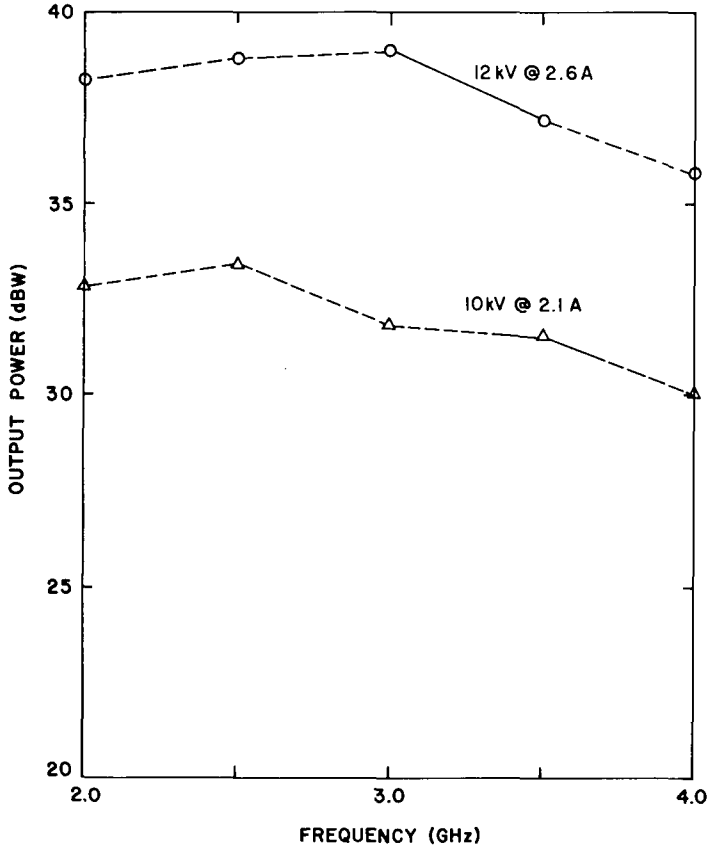


Fig. 15 — Output power as a function of frequency for two different beam conditions (tube 1). The available drive power (100 W) was capable of saturating the TWT only in the region indicated by the solid lines.

previously been operated up to 11.1 kW of peak RF power at a beam voltage of 13 kV and a cathode current of 3.2 A. The tube was rebuilt but mysteriously failed under very low duty operation.

The fifth tube failed during initial operation at low duty. Subsequent tests revealed that the AC circuit breaker feeding the trigger generator had overloaded and opened, which caused the modulator to change from 0.1% duty to full CW operation within 30 msec. The tube had not been prepared for CW operation, with the result that the helix was punctured. The tube was regunned and tested at low duty with the helix puncture sealed. Because of an inaccessible fluid leak between the input and attenuator sections, the tests were run using salt water in both the input and attenuator sections to suppress oscillations and either FC-43 or water in the output helix section. With a 1-*M* or lower concentration of salt in the attenuator section, voltage-tunable backward-wave oscillations were observed over the frequency range of 6.25-6.6 GHz as the voltage was varied from 11 to 14 kV, using FC-43 to cool the output helix section. With a 1.5-*M* salt concentration in the attenuator section, and FC-43 in the output helix, the saturated RF power output at 3 GHz could be varied from about 2 kW peak at 10 kV beam voltage to over 11 kW peak at 14.2 kV beam voltage. The use of water instead of FC-43 in the output helix reduced the saturated output power by an average of 11%.

The sixth tube was constructed with vane loading and a phase-velocity taper. This tube had rather poor beam transmission and slightly lower gain than the previous tubes. Due to the reduced circuit velocity at low frequency with vane loading, regenerative oscillations occurred below the output waveguide cutoff frequency, near 1.5 GHz, unless the salt concentration in the attenuator section was increased to over 2.5 moles. The output waveguide was replaced by a coaxial output coupler for low-duty operation. This permitted stable operation with a 1-*M* salt concentration in the attenuator section, which provided a 15-dB total attenuation through the tube at 3 GHz. However, the gain was still insufficient to permit broadband saturated power data to be taken with the available 100-W drive power source at the higher helix voltages where the output power is maximum. Some broadband data were obtained at the synchronous beam voltage of 11 kV where the gain was sufficient to saturate the tube over most of the S band. Typical results with FC-43 coolant in the output helix section were fundamental power output of 2.5 kW at 2 GHz, increasing to over 5 kW at 4 GHz. The saturated gain varied from 14 dB to 19 dB over this frequency range. The harmonic power separation (ratio of fundamental to harmonic power) was about 5 dB at 2 GHz, increasing to 20 dB at 3.5 GHz. Replacing FC-43 by water in the output helix section caused the saturated output power to decrease by about 10% in the frequency range from 3 to 4 GHz. The power output increased to over 7 kW at 3 GHz with 12 kV beam voltage applied. However, the TWT gain was insufficient to saturate the TWT at higher voltages with the available RF drive power.

During high-duty testing with the coax-to-waveguide adapter connected to the output window, the sixth tube delivered up to 2256 W of average power, measured calorimetrically, while operating at 50% RF duty and 100% beam duty. The helix voltage was 11.2 kV and the cathode current was 2.3 A. The total helix and body current was 0.11A without RF drive and increased to 0.33 A with RF drive. Thus the helix current was increased by about 0.22 A under drive, or about 10% of the total beam current was intercepted by the output helix circuit with 75 W of RF drive power. Water at an inlet pressure of about 25 psi was exited through the output window at a rate of 0.041 gpm, entering at 8.0°C and exiting at 35.9°C. This corresponds to a heat dissipation of 301W average for the water flowing through the output window. The tube was later destroyed by a sustained arc which melted a hole in the beryllia output window while the tube was operating at only about 1200 W of average RF power.

A mechanical model and cooling tests were made of a fluid-cooled helix designed to operate from 10 to 18 GHz. The inner diameter of the ceramic cooling support was too small to obtain enough cooling with FC-43 and too lossy to use water as a coolant. It was concluded that fluid cooling of helix TWTs is not worthwhile above 10 GHz and offers no advantages compared to conduction cooling with beryllia rods.

## CONCLUSIONS

Fluid cooling of helix traveling-wave tubes is an effective way of attaining high average and peak power operation over wide bandwidths. It provides approximately an order of magnitude more cooling, in the S-band frequency range, than the conventional conduction cooling. When it is accomplished by the methods described in this report, this cooling can be realized with fluid pressure drops that are practical.

The presence of fluid within the ceramic supports introduces additional RF losses over that due to skin effect losses in the helix and loss in the dielectric support. These losses can be minimized in the operating band of the tube at the input and output ends of the tube either by using a low-loss fluid such as FC-43 or by reducing the inner diameter of the ceramic supports. In the case of axial flow (and possibly for hybrid flow) the RF losses may be minimized by blocking the fluid from a selected number of ceramic supports near the helix output. In the attenuator region of the tube the RF losses can be increased to provide stability against regenerative oscillations through the use of a high-loss fluid, such as salt water, and by increasing the inner diameter of the ceramic support. The nature of the support is such that the RF losses increase rapidly with frequency above the operating band. This additional loss at the higher frequencies effectively suppresses the backward-wave oscillation which otherwise would limit the attainable power.

The need for many additional ceramic-to-metal seals required for this type of tube does not appear to be a formidable problem and did not cause any great difficulty with tube construction.

## ACKNOWLEDGMENT

The authors wish to thank Messrs. D. E. Cheville, H. L. Vess, L. V. Cheek, J. W. Dries, and E. A. Ehrmantraut for their work in TWT assembly, RF measurements, and other forms of assistance during this program.

## REFERENCES

1. J. A. Lucken, "Some Aspects of Circuit Power Dissipation in High Power CW Helix Traveling-Wave Tubes, Part I: General Theory," *IEEE Trans.* ED-16 (No. 9), 813-820 (Sep. 1969).

2. J. A. Lucken, "Some Aspects of Circuit Power Dissipation in High Power CW Helix Traveling-Wave Tubes, Part II: Scaling Laws," *IEEE Trans.* ED-16 (No. 9), 821-826 (Sep. 1969).

3. S. E. Webber, "1,000-Watt Traveling Wave Tube," *Electronics* 23, 100-103 (June 1950).

4. G. M. Clarke, "Power Limitations in Helix Traveling-Wave Tubes and the Application of Fluid Cooling," *Proc. IEE* 105, Pt. B Supplements, 446-454 (1958).

5. G. M. Clarke, "Experimental Traveling-Wave Tubes, C.W. Models for X-Band With Water-Cooled Helices," *Electron. Tech.* 38, No. 2, 38-45 (Feb. 1961).

6. H. D. Arnett, S. T. Smith, and L. M. Winslow, "Design Concepts for Dual-Mode Traveling Wave Tubes," NRL Memorandum Report 2599, May 1973.

# Appendix A
# BRAZING TECHNIQUES

Two different methods have been used to join the ceramic tubes to the helix. Both methods begin with the copper tubing having been formed in the shape of a helix by winding the tubing onto a threaded mandrel (Fig. A1). The mandrel is precision ground and serves the dual purpose of determining helix dimensions and preventing tubing collapse during the helix winding operation.

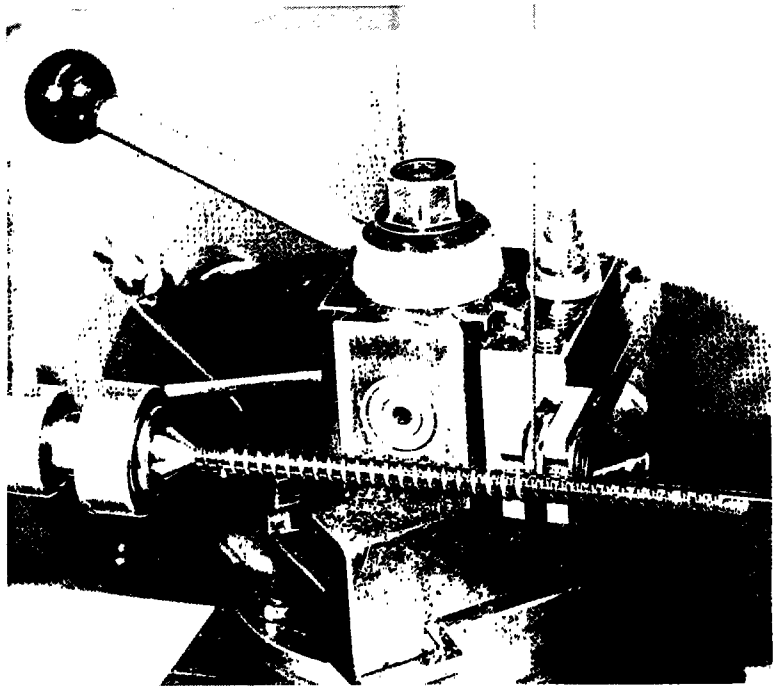

Fig. A1 — The S-band helix being wound on its mandrel

In the first brazing method, called the taper brazing technique, holes are drilled in the helix at each half turn using an electric discharge machining (EDM) technique. The helix, while still on the threaded mandrel, is mounted in a fixture and placed in the EDM tank. With a microscope and a micrometer drive on the tank, the machining electrode can be properly located on the helix turns and holes can be accurately drilled without having the tubing collapse or burrs form around the edges of the hole. The machining electrode is a brass rod 0.042 in. in diameter that drills a hole about 0.046 in. in diameter. The tank fluid is tetraethylene glycol, and the power source is a 500-V, 300-mA DC power supply with a series resistor of 1500 ohms and with a 0.03-$\mu$F capacitor connected across the electrodes. Next, the helix is chemically cleaned, then annealed in the hydrogen furnace. The helix is then cut to length and removed from the mandrel.

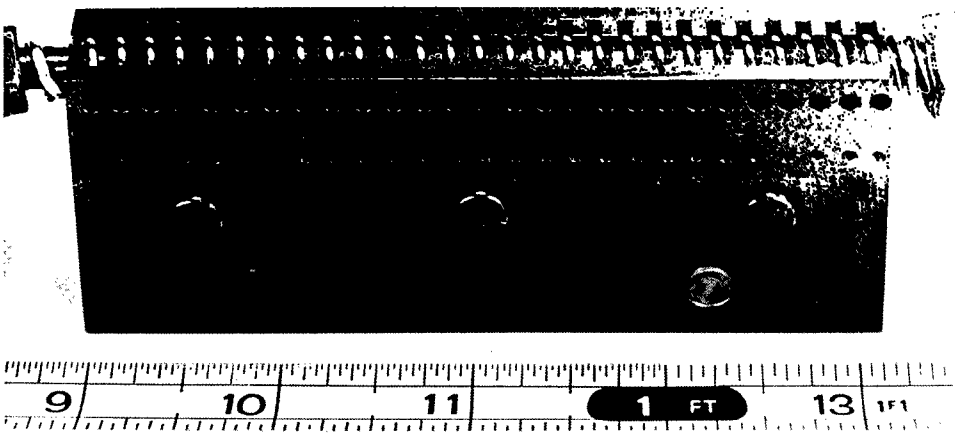


Fig. A2 — A section of helix in the brazing fixture for ceramic brazing

The ceramic tubes used in this helix assembly are Alsimag 771, a 94% alumina ceramic. These tubes are 0.250 in. long and have an outer diameter of 0.065 in. Some of the tubes have an inner diameter of 0.020 in., and some have an inner diameter of 0.032 in. Those with the larger inner diameter are used in the attenuator section of the tube, and those with the smaller inner diameter are used for the rest of the helix. The ceramic tubes have a 16° taper ground on one end and a chamfer on the other. The tubes are metallized on the taper, then follows a clean band of about 0.060 in., and a metallized band covers the remainder of the tube. The length of the clean band corresponds roughly to the distance between the helix and barrel. The metallizing is moly-manganese, which was selected as the best known and most reliable technique.

The ceramic tubes are brazed to the helix using a stainless steel fixture which has been designed to support the helix turn by turn and to position the ceramic tubes accurately. Figure A2 shows this fixture with the helix inserted. The slots that support the helix can be seen at the top of the fixture. The holes near the top of the fixture position the ceramic tubes. The helix is clamped inside this fixture, and the ceramic tubes, with rings of 0.010-in. gold-copper brazing alloy wire mounted on the tapers, are inserted in the large holes near the top. Stainless steel bushings are inserted in each hole to center the ceramic tubes, and flat stainless steel springs are mounted on the outside of the fixture to hold each ceramic tube in contact with the helix. The assembly is then brazed in the hydrogen furnace under carefully controlled conditions to avoid erosion of the copper helix. Figure A3 shows a section of the helix as it appears after removal from the brazing fixture. This photograph also shows the typical smooth mandrel used to support the helix in the final barrel braze. This mandrel is a stainless steel rod with flats ground on the sides near the braze joints. These flats allow slight distortion in the helix as the helix and barrel assembly cools after being brazed and make it possible to remove the mandrel without damage to the helix.

Fig. A3 — The taper-brazed seals

A second method, which is called the butt brazing method, has more recently been used to join the ceramic tubes to the helix. In this method the ceramic tubes are prepared by grinding a small chamfer on each end. These are shown on the right in Fig. A4. One end of the ceramic tube can be contoured to fit the curvature of the helix if so desired, but this has never been done. The ceramic tubes are chemically cleaned, and then bands of heat-shrinkable tubing are positioned so as to mask the clean brazed area. These are shown in the middle of Fig. A4. The clean band on these ceramic tubes has been increased to 0.125 in. because the barrel diameter has been increased in the more recently constructed traveling wave tubes. The ceramic tubes are sprayed with moly-manganese, air dried, and the plastic bands removed. The plastic bands can be removed easily by scoring them with a razor blade and then heating them with a hot-air gun. In Fig. A4 the metallized ceramic tubes are shown on the left with solder rings made from 0.008-in. gold-copper brazing alloy.

These ceramic tubes are brazed to the helix using the same brazing fixture and the same techniques just described for the taper brazing method. Figure A5 shows a section of helix constructed by the butt brazing method. At this point an opening from each ceramic tube into the helix must be provided. With the helix assembly still in the brazing fixture, holes can be drilled through the 0.005-in. helix wall by going into each ceramic tube with a No. 70 or 78 drill held in a pin vise. Care must be taken to avoid breaking the small drills and thus blocking the flow through the helix.

The butt-brazing technique has yielded a 25% reduction in time required for preparing ceramic tubes and assembling helices. The resulting seals also have greater strength and better vacuum integrity compared to those made by the first method.

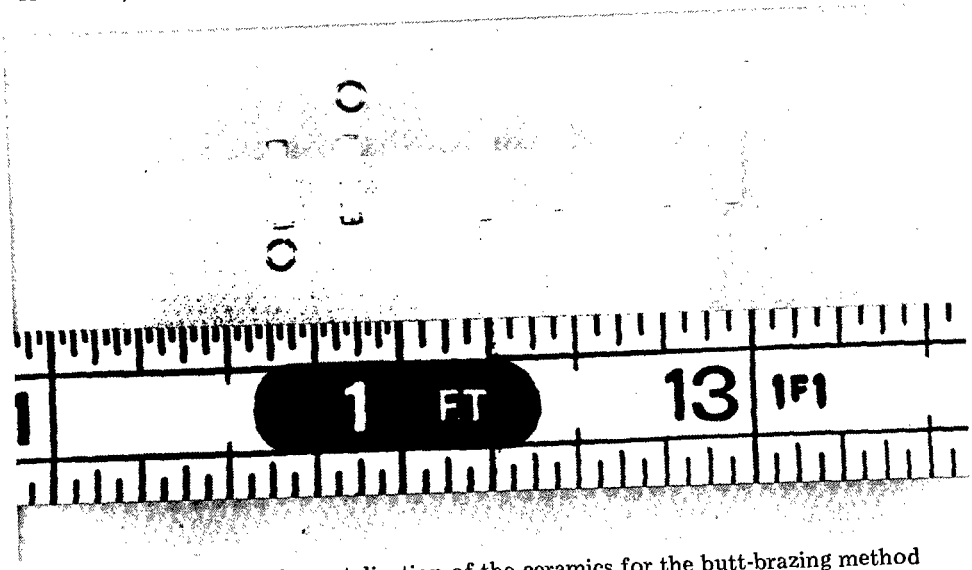


Fig. A4 — Steps in the metalization of the ceramics for the butt-brazing method

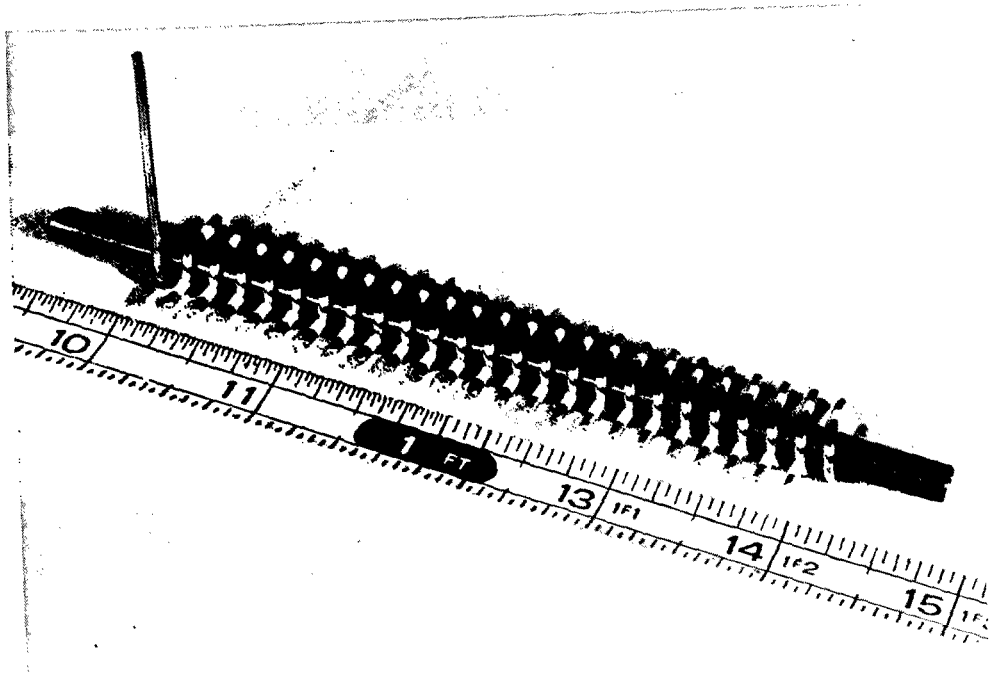


Fig. A5 — The butt-brazed seals

# Appendix B
# BASIC COOLING DESIGN EQUATIONS

For a given coolant flow configuration, the cooling fluid passes through a series of ducts, bends, contractions, or other flow discontinuities. Each section of the coolant flow path may have associated with it a pressure drop or a temperature rise which is a function of the local flow rate, the geometry, the physical properties of the cooling fluid, and, of course, the power absorbed in that section. The total pressure or temperature at any position in the cooling system is then determined by the summation of the various pressure and temperature changes along the coolant flow path.

In this appendix, simplified working equations are developed for the pressure and temperature increments of the subelements which make up the complete cooling system, starting from the basic heat and fluid-flow relations available in the literature [B1-B4]. These are combined in Appendix C for the calculation of the total pressure drop and the maximum temperature for several useful cooling configurations of the fluid-cooled TWT.

Some of the units used in the literature on heat flow and fluid flow have different dimensions from those preferred by TWT designers and others in the electronics industry. The symbols, together with their dimensions, are given in the list of symbols. In the final working equations power is expressed in watts, temperature in degrees C, fluid flow in gallons per minute, pressure in pounds per square inch, and all distances are expressed in inches. In some of the intermediate equations different dimensions are used; when this occurs, the symbol carries a prime, and the dimensions are those specified in the list of symbols.

## The Reynolds Number and Transition Flow Rate

Maximum cooling occurs if the fluid flow is turbulent rather than laminar. Turbulent flow causes the fluid near the duct wall to be mixed more rapidly with the bulk of the fluid away from the duct wall and therefore ensures a more effective heat transfer from the inner wall of the tubing to the cooling fluid. The flow rate at which the transition from laminar to turbulent flow occurs is determined by the dimensionless Reynolds number $R_D$, given by

$$R_D = \frac{V'D'\rho}{\mu} = \frac{4}{\pi}\frac{F'}{D'}\frac{\rho}{\mu} . \tag{B1}$$

In Eq. (B1) $V'$ is the average velocity of the fluid, $F'$ is the volume flow rate, $D'$ is the pipe diameter, $\rho$ is the fluid mass density, and $\mu$ is the viscosity. Since $R_D$ is dimensionless, any consistent set of units can be used on the right-hand side of the equation.

In straight ducts the transition from laminar to turbulent flow occurs at a critical flow rate $F_T$, corresponding to a Reynolds number [B1-B3] of about 2300. Then, turbulent flow requires that

$$F > F_T = 0.30\left(\frac{\mu}{g}\right)D, \tag{B2}$$

where $F$ and $F_T$ are expressed in gallons per minute if $D$ is the duct equivalent diameter in inches, $\mu$ is the fluid viscosity in pounds per hour-foot, and $g$ is the specific gravity of the coolant relative to water at 4°C. A duct entrance or similar flow disturbance will set up turbulence which will generally continue for several duct diameters if the flow is less than the threshold value. For fluid flowing in a coiled duct, such as a helix turn, the transition Reynolds number is increased [B2]. The threshold flow rate is then given approximately by

$$F_T = 0.30(1.0 + 2.7e^{-0.02a/D})\left(\frac{\mu}{g}\right)D, \tag{B3}$$

where $a$ is the helix radius and $D$ is the inner diameter of the helix tubing.

**Heat Inputs**

The heat inputs to the cooling system for the fluid-cooled helix TWT arise from three sources. These are (a) RF losses, (b) beam interception, and (c) irreversible pressure losses. The RF losses usually are the largest heat input source if the TWT has a well-designed focusing system.

It is convenient for analysis to separate the RF losses per ceramic into two parts. That is,

$$\tau = \tau_h + \tau_c, \tag{B4}$$

where

$\tau$ = the total RF loss in decibels in one half turn of the helix,

$\tau_h$ = the helix $I^2R$ loss in one half helix turn,

$\tau_c$ = RF loss inside the fluid-filled ceramic support.

Usually the RF loss inside the dielectric material of the ceramic support is negligible, and most of the ceramic RF loss is dissipated directly in the fluid. If the heat dissipation per half turn caused by RF losses is given by $P_t$, then

$$P_t = (1 - 10^{-\tau/10})P_{RF}, \tag{B5}$$

or for small $\tau$,

$$P_t = 0.23\tau P_{\mathrm{RF}}, \tag{B5a}$$

giving

$$P_c = 0.23\tau_c P_{\mathrm{RF}}, \tag{B5b}$$

and

$$P_h = 0.23\tau_h P_{\mathrm{RF}}. \tag{B5c}$$

The error in using the small $\tau$ approximation is less than 5% for $\tau$ less than 0.44 dB.

For the examples calculated in this report $\tau_c$ is about 0.10 dB per ceramic for the 0.032-in. I.D. support ceramics with water used as the cooling fluid. The loss is assumed to vary directly with the conductance of the fluid column for other cases. The RF loss of the helix $\tau_h$ is estimated to be a maximum of 0.10 dB/wavelength for the 0.060-in. O.D. (0.050-in. I.D.) helix and is assumed to vary inversely as the helix duct diameter. Then, for four helix turns per wavelength (eight ceramics per wavelength),

$$\tau_h = \frac{0.10}{8} = 0.0125 \text{ dB per ceramic.}$$

In the previous equations, $P_{\mathrm{RF}}$ is the peak RF power at the position where the heat dissipation is calculated. This may be increased significantly if the power reflected from the output coupler is high. At the output coupler the reflected RF power is

$$P_R = r^2 P_F = \frac{r^2 P_0}{(1 - r^2)}, \tag{B6}$$

where

$r$ = the voltage reflection coefficient at the output coupler,

$P_0$ = the net RF output power,

$P_F$ = the power in the amplified forward wave,

$P_R$ = the reflected RF power.

$P_F$ can be determined at any axial position on the circuit from the signal growth rate and the RF drive power relative to saturation. $P_R$ at any position is equal to its value at the output, reduced by the cold circuit attenuation in front of the output coupler.

The average and maximum heat dissipations are given by

$$(P_{\mathrm{RF}})_{\mathrm{ave}} = P_F + P_R, \tag{B7}$$

and

$$(P_{RF})_{max} = (P_F^{1/2} + P_R^{1/2})^2. \tag{B8}$$

It is apparent from Eqs. (B5), (B7), and (B8) that a large derating factor (up to a maximum of 4:1 at the output) is required if the output coupler mismatch is high.

The total heat input power $P_i$ caused by beam interception in the output circuit may be expressed as

$$P_i = k_b \Delta I_h E_h, \tag{B9}$$

where $E_h$ is the helix voltage, $\Delta I_h$ is the increase in helix current interception under RF drive, and $k_b$ is a constant which is less than unity. The factor $k_b$ accounts for the fact that the average kinetic energy of the intercepted electrons is much lower than their initial energy, as a result of the energy extracted during the interaction process. The very slowest electrons (which cannot be focused) will be intercepted first, and $k_b$ will be a function of the TWT interaction efficiency and the quality of the beam focusing system. When expressed as a fraction of the initial beam power $P_b$ and the total beam current $I_b$, Eq. (B9) becomes

$$\frac{P_i}{P_b} = k_b \frac{\Delta I_h}{I_b}. \tag{B9a}$$

It is estimated that $k_b$ may vary from 0.2 or less with good beam focusing to 0.4 or more with poor focusing, and $\Delta I_h/I_b$ may vary from 0.5% to 5.0%. Thus, from 0.1% to 2% of the initial beam energy may be converted to heat near the output coupler, depending on the quality of the beam focusing system. With a confined-flow solenoid focusing system, the heat dissipation caused by beam current interception may be quite small in comparison to RF heating. The axial or radial distribution of beam-current interception is not subject to accurate determination. A derating factor may be applied to a specific design to account for the increased heat generated by beam interception.

From simple energy considerations the power required to force the cooling fluid through the helix is given by

$$P' = F'\Delta p', \tag{B10}$$

where $F'$ is the flow rate and $\Delta p'$ is the pressure drop. This power is converted inside the cooling system to either (a) frictional fluid losses which increase the fluid temperature or (b) kinetic energy of the moving fluid. For the complete cooling system the initial and final fluid velocities are essentially zero. For a total pressure drop of 50 psi and a flow rate of 0.04 gpm per ceramic (typical for the cross-flow configuration with 0.020-in. I.D. support ceramics), the heat dissipation generated by irreversible pressure losses is calculated from Eq. (B10) to be only 0.87 W in one half turn of the helix. About one-fourth of this occurs in converting the kinetic energy of the exiting fluid into heat, and thus has no effect on heating the fluid inside the helix. The remaining heat generated by irreversible pressure losses inside the helix assembly will raise the temperature of the fluid by 0.06°C (if it is water) and is insignificant in comparison with other heat sources. It is neglected in the cooling analysis.

### Temperature Rise of the Cooling Fluid

From the definition of heat capacity, a quantity of heat $Q$ absorbed by the fluid will cause its temperature to increase by an amount given by

$$\Delta T' = \frac{Q}{mc}$$

where $Q$ is quantity of heat in Btus, $m$ is the mass of fluid in pounds, $c$ is the specific heat in Btus per pound per degree Fahrenheit, and $\Delta T'$ is the temperature change in degrees Fahrenheit. When this is converted to a per unit of time basis the working equation

$$\frac{\Delta T}{P_t} = \frac{3.78 \times 10^{-3}}{cgF} \tag{B11}$$

results. Here $\Delta T$ is the fluid temperature rise (°C), $P_t$ is the input thermal power (W), and $F$ is the coolant flow rate.

Within the support ceramics, most of the heat is generated directly in the cooling fluid, and the value of $P_c$ determined by Eq. (B5b) can be used in Eq. (B11) to determine the temperature rise of the fluid as it passes through the support ceramics. Similarly, $P_h$ from Eq. (B5c) is used in Eq. (B11) to determine the temperature rise of the fluid in passing through one half turn of the helix.

### Helix Duct Temperature Rise

Heating due to helix RF losses or beam interception is generated on the surface of the helix or within essentially one skin depth of the helix surface and is transferred by conduction to the inner surface of the helix tubing. The temperature drop associated with heat flow through the helix wall is negligible.

Inside the helix tubing there is a rather large temperature drop between the inner wall of the helix and the bulk of the fluid. This is termed the duct temperature drop $\Delta T_D$, and its value depends upon whether the coolant flow is laminar or turbulent.

For *turbulent flow*, Scott [B1, p. 114] gives the working equation

$$\frac{\Delta T_d}{P_t} = 0.246 \left( \frac{\mu^{.4}}{C^{.4} k^{.6} g^{.8}} \right) \frac{D^{.8}}{F^{.8} L} \quad , \tag{B12}$$

where $k$ is the thermal conductivity of the coolant (Btu/hr ft °F) and $L$ is the length of the cooling duct (inches). The other terms have been defined previously.

Equation (B12) applies to a long straight tube. The probable effect of the helix curvature is to reduce the duct temperature below the value given by Eq. (B12). No data appear to be available on this for liquids, but McAdams [B3, p. 228] indicates that for

gases flowing in a turbulent condition in a helical coil the temperature drop should be divided by the factor $(1 + 1.75D/a)$. Since actual data for liquids are not available, all calculations for duct temperature rises in the helix for turbulent flow have been based on Eq. (B12).

The working equation, given by Scott [B1, p. 114] for the case of *laminar flow* is

$$\frac{\Delta T_d}{P_t} = 0.20 \frac{1}{C^{.33} k^{.67} g^{.33}} \frac{1}{L^{.67} F^{.33}} . \tag{B13}$$

**Pressure Drop in Ducts**

The pressure drop for a straight round duct of length $L$ and diameter $D$ is given by McAdams [B3, p. 145] as

$$\Delta p' = 4f \frac{L}{D} \frac{\rho V'^2}{2g_c} \tag{B14}$$

where $g_c = 32.17$ ft/sec$^2$ is the acceleration of gravity and $f$ is a friction factor which depends on the Reynolds number and the roughness of the duct wall surface. The factor $(\rho V'^2/2g_c)$ in Eq. (B14) has the dimensions of pressure and is commonly referred to as velocity head. It is also seen to be equal to the average kinetic energy per unit volume of the moving fluid. The velocity head is given, in convenient units, by

$$VH = 1.124 \times 10^{-3} \frac{gF^2}{D^4} . \tag{B15}$$

The dimensions of $VH$ in Eq. (B15) are pounds per square inch.

For well-developed *laminar flow* in incompressible fluids, $f$ is given by McAdams [B3, p. 149] as

$$f = \frac{16}{R_D} , \tag{B16}$$

which is applicable for any degree of duct surface roughness. Using Eqs. (B14), (B15), (B16), and (B1) results in the equation obtained for pressure drop in round ducts for laminar flow:

$$\Delta p = 9.4 \times 10^{-6} \mu \frac{FL}{D^4} . \tag{B17}$$

For *turbulent flow* in straight smooth ducts such as drawn tubing, McAdams [B3, p. 155] gives the approximate expression for $f$ as

$$f = \frac{0.046}{(R_D)^{0.2}} , \tag{B18}$$

which is said to be accurate to about ± 5% for $5{,}000 < R_D < 200{,}000$. The expression for pressure drop in smooth ducts and turbulent flow is, therefore,

$$\Delta p = 3.46 \times 10^{-5}(g^{.8}\mu^{.2}) \frac{F^{1.8}L}{D^{4.8}} . \tag{B19}$$

For turbulent flow in helix bends the pressure drop is given in Ref. B2, Sec. 403 as

$$\Delta p' = C_{B90}C_\theta \frac{\rho V'^2}{2g_c} . \tag{B20}$$

The term $C_{B90}$ is the pressure loss in terms of the fraction of a velocity head lost in a 90° bend, and it is a function of the ratio of helix diameter to duct diameter, $a/D$. For the helix tubing $a$ = 0.154 in., and $D$ = 0.050 in.; thus $a/D$ = 3.08, and the value of $C_{B90}$ given in Ref. B2 is about 0.2. $C_\theta$ is a factor by which $C_{B90}$ is to be multiplied for other than 90° bends, and it is about 1.6 for a 180° bend. In convenient units Eq. (B20) may be written as

$$\Delta p = 1.124 \times 10^{-3}C_{B90}C_\theta \frac{gF^2}{D^4}$$

$$\Delta p = 1.124 \times 10^{-3}C_B \frac{gF^2}{D^4} . \tag{B21}$$

This equation includes the effect of friction in the bend, so the bend length should not be included when calculating the pressure drop produced by friction in the rest of the duct system.

### Pressure Change Caused by Change in Duct Diameter

Large pressure changes occur in the fluid-cooled TWT at entrances to ducts where the diameter of the flow changes. These pressure changes are strongly dependent on the geometry at the disturbance and may be calculated in terms of a pressure-loss coefficient $C_D$, which gives the static pressure change in terms of the number of velocity heads.

Following normal convention the algebraic sign of the pressure change is chosen such that a drop in pressure in the direction of flow has a positive numerical value, and a rise in pressure has a negative numerical value. The pressure used here is the static pressure, which is related to the total pressure at any location by

$$p(\text{total}) = p(\text{static}) + 1.124 \times 10^{-3} \frac{gF^2}{D^4} . \tag{B22}$$

Thus the total pressure at any location exceeds the static pressure by the velocity head. The total pressure always decreases in the direction of flow, while the static pressure may increase if the fluid velocity is reduced by expansion into a larger duct diameter.

For fluid flow in contractions or expansions from one duct diameter to another, the pressure drop is given in terms of a contraction coefficient $K_c$ or by an expansion coefficient $K_e$ by General Electric [B2] and by Kraus [B4], as

$$\Delta p = 1.124 \times 10^{-3} \frac{gF^2}{D_2 4} \left\{ K_c + \left[ 1 - \left( \frac{D_2}{D_4} \right)^4 \right] \right\} \tag{B23}$$

for flow contractions, and as

$$\Delta p = 1.124 \times 10^{-3} \frac{gF^2}{D_2 4} \left\{ K_e - \left[ 1 - \left( \frac{D_2}{D_4} \right)^4 \right] \right\} \tag{B24}$$

for flow expansions. In both Eqs. (B23) and (B24), $D_2$ is the smaller of the two diameters, $K_c$ or $K_e$ represent the unrecoverable portion of the pressure drop, and the portion $[1 - (D_2/D_1)^4]$ for contractions is the increase in the velocity head which may be partially recovered by expansion of the fluid downstream.

For convenience of calculation the terms within braces in both Eqs. (B23) and (B24) are combined into a single static pressure coefficient $C_D$, so that the static pressure drop is given by

$$\Delta p_s = 1.124 \times 10^{-3} C_D \frac{gF^2}{D_2^4} . \tag{B25}$$

Equation (B25) is a general expression for pressure drop for all types of flow constrictions when the flow is turbulent. The coefficient $C_D$ is tabulated in Ref. B2 (Sec. 405.3, p. 1) for many types of flow constriction which may occur in fluid-cooled helix TWTs. For fluid flowing more slowly than the indicated Reynolds number, range $C_D$ increases very slowly with decreasing flow rate, and the values given can be used with fair accuracy over the complete range of turbulent flow.

Suitable values of $C_D$ for laminar flow conditions are difficult to determine, but they are not often needed for the fluid-cooled helix. Krauss [10 pp. 143-145] suggests the approximate selections

$$C_D \text{ (laminar flow)} \approx C_D \text{ (turbulent flow)} \tag{B26a}$$

for expansions, and

$$C_D \text{ (laminar flow)} \approx C_D \text{ (turbulent flow)} + 0.50 \tag{B26b}$$

for contractions.

For the hypothetical ideal fluid with frictionless fluid flowing from an infinite fluid reservoir into a duct, $C_D = 1.0$ and all of the pressure drop is converted to a velocity head (kinetic energy). For real fluids flowing through tapered or rounded entrances from a fluid reservoir, $C_D$ is usually in the range of 1.04 to 1.13. For an entrance with sharp square edges, $C_D$ has a value of 1.45 for turbulent flow and about 1.95 for laminar flow. $C_D \approx 0$ at the exit from a duct into a reservoir. The latter values were used to calculate the pressure drops at the junctions between the support ceramics and the helix or the fluid reservoirs for the fluid-cooled helices.

## REFERENCES

B1. W. A. Scott, *Cooling of Electronic Equipment*, Wiley, New York, 1974.

B2. "Heat Transfer and Fluid Flow," General Electric Company, Schenectady, N.Y., 1970.

B3. W. H. McAdams, *Heat Transmission*, 3rd ed., McGraw-Hill, New York, 1954.

B4. A. D. Kraus, *Cooling Electronic Equipment*, Prentice-Hall, Englewood Cliffs, N.J., 1965.

## Appendix C
## COOLANT FLOW AND TEMPERATURE RISE FOR FLUID-COOLED HELIX CONFIGURATIONS

The basic cooling design equations developed in Appendix B are combined here to determine the total coolant flow rate and temperature rise as functions of the pressure drop, type of cooling fluid, and dimensions of the helix assembly for several flow configurations. After the general flow equations for a general coolant fluid and geometry are developed, the procedure is illustrated by the example of the S-band fluid-cooled helix with water as the coolant. The appropriate data are

$2a$ = 0.308 in. = helix average diameter

$D_h$ = helix duct inner diameter (inches)

$D_c$ = ceramic duct inner diameter (inches)

$L_h \approx \pi a$ = 0.484 in. = length of helix ducts between ceramic supports

$L_c$ = 0.250 in. = length of ceramic supports

$\tau_h$ = 0.0125 $(0.050/D_h)$ = the RF skin loss in one half turn of the helix (dB)

$\tau_c$ = 0.10 $(D_c/0.032)^2$ = the RF loss due to the fluid in each ceramic (dB).

The fluid used was water at 20°C inlet temperature. It is assumed that the power is limited by the onset of boiling either at the inside surface of the helix or in the exit ceramics. For this example, the pressure drop is taken to be 50 psi, and the voltage reflection coefficient at the output coupler is assumed to be zero.

### Cross Flow

The cross-flow configuration is illustrated schematically in Fig. C1. Coolant from a reservoir enters through a set of tubular ceramic supports on one side of the helix structure, splits into two flow paths in flowing through the helix, and exits through the opposite set of support ceramics. By symmetry, the flow rate through an individual helix section is one-half the flow rate through a ceramic; i.e., for cross flow

$$F_h = 0.5\, F_c, \tag{C1}$$

where $F_h$ is the fluid flow rate in the helix (gpm) and $F_c$ is the fluid flow rate in the ceramic (gpm).

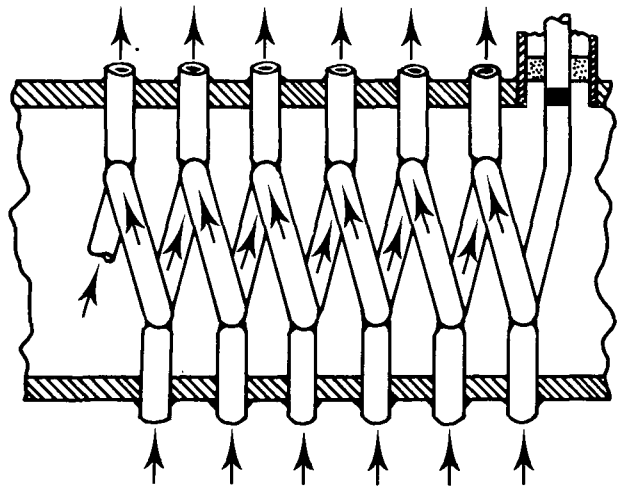

Fig. C1 — Cross flow configuration

The major pressure drop for cross flow occurs where the fluid enters an inlet ceramic and again where the fluid enters an exit ceramic. If square edges at the ceramic entrances are assumed, the static pressure drop at each entrance is about 1.45 velocity heads when the flow inside the ceramic is turbulent and 1.95 velocity heads when the flow is laminar. Thus from Eq. (B25) the pressure drop at each of these ceramics is

$$\Delta P_e \text{ (ceramic)} = 2.19 \times 10^{-3} \frac{gF_c^2}{D_c^4}, \quad \text{for } F_c < 0.30 \left(\frac{\mu}{g}\right) D_c \tag{C2}$$

and

$$\Delta P_e \text{ (ceramic)} = 1.63 \times 10^{-3} \frac{gF_c^2}{D_c^4}, \quad \text{for } F_c > 0.30 \left(\frac{\mu}{g}\right) D_c. \tag{C3}$$

The duct pressure drop in a ceramic is given by Eqs. (B17) and (B19) for laminar and turbulent flow, respectively. The results are

$$\Delta P_d \text{ (ceramic)} = 9.4 \times 10^{-6} \mu F_c L_c D_c^4, \quad \text{for } F_c < 0.30 \left(\frac{\mu}{g}\right) D_c \tag{C4}$$

and

$$\Delta P_d \text{ (ceramic)} = 3.46 \times 10^{-5} (g^{.8} \mu^{.2}) \frac{F_c^{1.8} L_c}{D_c^{4.8}} \quad \text{for } F_c > 0.30 \left(\frac{\mu}{g}\right) D_c. \tag{C5}$$

Other pressure drops are quite small compared to those considered above. The duct pressure drop in the helix tubing is quite low for practical cases. The static pressure losses at the exit from the inlet and outlet ceramics are negligible. Also the turn losses at the

junctions between helix and ceramics are neglected because the flow velocity in the helix is relatively low compared to that in the ceramics for practical cases.

Since there are two ceramics involved in cross flow, the pressure drop from inlet reservoir to outlet reservoir is

$$\Delta p = 4.38 \times 10^{-3} \frac{gF_c^2}{D_c^4} + 1.88 \times 10^{-5} \frac{\mu L_c F_c}{D_c^4}, \quad \text{for } F_c < 0.30 \left(\frac{\mu}{g}\right) D_c \tag{C6}$$

and

$$\Delta p = 3.26 \times 10^{-3} \frac{gF_c^2}{D_c^4} + 6.92 \times 10^{-5} (g^{.8}\mu^{.2}) \frac{L_c F_c^{1.8}}{D_c^{4.8}} \quad \text{for } F_c > 0.30 \left(\frac{\mu}{g}\right) D_c. \tag{C7}$$

For the S-band TWT, when water is the coolant ($g = 1$, $\mu = 2.3$ lb/hr ft), these equations become

$$\Delta p = 4.38 \times 10^{-3} \frac{F_c^2}{D_c^4} + 1.08 \times 10^{-5} \frac{F_c}{D_c^4}, \quad \text{for } F_c < 0.69 D_c \tag{C6W}$$

and

$$\Delta p = 3.26 \times 10^{-3} \frac{F_c^2}{D_c^4} + 2.04 \times 10^{-5} \frac{F_c^{1.8}}{D_c^{4.8}}, \quad \text{for } F_c > 0.69 D_c. \tag{C7W}$$

Flow rates computed from these equations are slightly lower than the measured values given in Fig. C2.

The maximum RF power capability is determined by the helix and fluid RF losses, beam interception, total applied pressure, maximum allowed coolant temperature, RF drive power (or power distribution on the helix), and the load mismatch. It will be assumed that the other sources of heat are negligible compared to the helix and fluid RF losses.

The RF losses vary with duct dimensions as indicated at the beginning of this appendix. The heat dissipation caused by electron beam interception on the helix was discussed in Appendix B. Including these two effects results in values for the power dissipated in a helix half turn $P_h$ and in a ceramic $P_c$ of

$$P_h = \left(\frac{1.44 \times 10^{-4}}{D_h} + 0.15 \frac{\Delta I_h}{I_b}\right) P_{RF} \tag{C8}$$

and

$$P_c = 22.5 D_c^2 P_{RF}. \tag{C9}$$

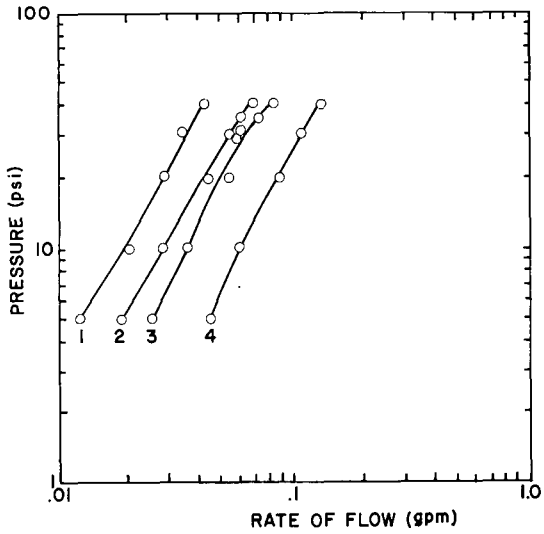


(a) Measurements made using a 6-turn helix and 11 ceramics with water as a coolant
1—Average cross flow per half turn using 0.050-in. I.D. tubing and 0.032-in. I.D. ceramics
2—Hybrid flow out the end of helix using 0.040-in. I.D. tubing and 0.020-in. I.D. ceramics
3—Hybrid flow out the end of helix using 0.050-in. I.D. tubing and 0.032-in. I.D. ceramics
4—Axial flow using 0.050-in. I.D. tubing and 0.032-in. I.D. ceramics

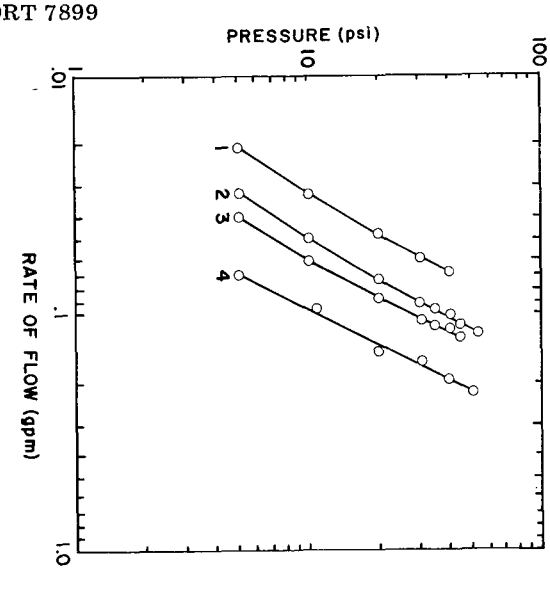


(b) Measurements made using a 6-turn helix and 11 ceramics with FC-43 as a coolant
1—Average cross flow per half turn using 0.050-in. I.D. tubing and 0.032-in. I.D. ceramics
2—Hybrid flow out the end of helix using 0.040-in. I.D. tubing and 0.020-in. I.D. ceramics
3—Hybrid flow out the end of helix using 0.050-in. I.D. tubing and 0.032-in. I.D. ceramics
4—Axial flow using 0.050-in. I.D. tubing and 0.032-in. I.D. ceramics

Fig. C2 — Measured flow rates for an S-band fluid-cooled helix. The average helix diameter was 0.307 in. and there were 6 turns per inch

The second term inside the parentheses of Eq. (C8) accounts for the heat dissipation in a helix half turn at the TWT output due to beam interception. The numerical value of the constant is based on the assumption that the beam interception is distributed uniformly over the last four helix turns at the output, that the electronic efficiency is 25%, and that $k_b = 0.3$.

The RF power will be limited by the onset of boiling either at the exit ceramic or inside the helix. Using Eqs. (B11), (C8), and (C9) and assuming 20°C for the water inlet temperature, we find that boiling will occur at the exit ceramic when the RF power is given by

$$(P_{RF})_{max} = \frac{470\,F_c}{D_c^2 + \dfrac{6.40 \times 10^{-6}}{D_h} + 6.66 \times 10^{-3}\,\dfrac{\Delta I_h}{I_b}} \qquad \text{(C10)}$$

where $F_c$ can be calculated using Eq. (C6W) or (C7W). For some cases $F_c$ can be read from Fig. C2. The computed value of $F_c$ gives a lower value of RF power than the

experimental value of $F_c$. For instance, with $D_h$ = 0.050 in. and $D_c$ = 0.020 in., the computed value of $F_c$ gives an RF power limitation due to boiling at the exit ceramics of about 39 kW without beam interception and about 31 kW with 2% interception.

In most, if not all, cases of interest, boiling first occurs at the inner surface of the helix. In calculating the temperature increment between the inside surface of the helix and the bulk temperature of the fluid in the helix, we must determine whether the flow in the helix is turbulent or laminar. Based on Eq. (B3) and the parameters of the S-band TWT, the threshold flow rate in ceramics is given by

$$F_c = 5.11\, D_h - 1.15 \times 10^{-2}.$$

For laminar flow Eq. (B13) is used to give the maximum RF power as

$$(P_{RF})_{max} = \frac{941\, F_c}{D_c^2 + \left(\frac{1.29 \times 10^{-3}}{D_h} + 1.35\, \frac{\Delta I_h}{I_v}\right)(F_c^{.67} + 9.9 \times 10^{-3})} \qquad \text{(C11)}$$

for $F_c < 5.11\, D_h - 1.15 \times 10^{-2}$. For turbulent flow Eq. (B12) leads to the result that

$$(P_{RF})_{max} = \frac{941\, F_c}{D_c^2 + \left(\frac{1.28 \times 10^{-5}}{D_h} + 1.33 \times 10^{-2}\, \frac{\Delta I_h}{I_b}\right)(1 + 164\, D_h^{.8} F_c^{.2})} \qquad \text{(C12)}$$

for $F_c > 5.11\, D_h - 1.15 \times 10^{-2}$.

For the example used above ($D_h$ = 0.050 in., $D_c$ = 0.020 in.), the calculated flow is laminar and the maximum power calculated from Eq. (C11) is 10.8 kW with no interception and 5.6 kW with 2% interception. This is less than the 39 kW computed for exit ceramic boiling. Therefore, for this example, the maximum power is limited by boiling at the inner surface of the helix. At this maximum power level, by far the largest temperature drop is the duct temperature drop between the surface of the helix and the bulk temperature of the fluid. For this example, it is 66.2°C when no interception was assumed.

Equations (C10), (C11), and (C12) have been used together with flow rates computed from Eqs. (C6W) or (C7W) to compute the maximum power to be expected for the S-band TWT for a wide range of values of ceramic diameter, helix tubing diameter, and beam interception. The results are plotted in Figs. C3a through C3c. For all of these plots the applied pressure was taken as 50 psi. Over all of the range of interest the flow in the helix is computed to be laminar, and the power is limited by boiling inside the helix. For larger than practical ceramic sizes, the flow is computed to be turbulent, and the abrupt power limit shown in Fig. C3 results from boiling of the coolant in the exit ceramic at that level.

Because of the manner in which the fluid is injected into the helix, the flow will be turbulent at the point of entrance, and this turbulence will persist for at least a fraction

of a half turn. It is then possible that the flow may remain turbulent. The maximum power to be expected under turbulent conditions has been computed for the same parameters above and is plotted in Figs. C4a through C4c. In the range of interest a slightly higher maximum power is expected for turbulent flow over laminar flow.

The requirement of large $D_c$ and large $D_h$ for maximum power is unfortunate. Because the RF loss is proportional to $D_c^2$, large $D_c$ would result in substantial reduction in the TWT conversion efficiency. This effect is quite significant even for $D_c$ = 0.020 in. with water cooling. Also, there is a limit to the helix tubing diameter because of TWT RF design considerations. As the helix tubing diameter is increased, there is less space available for the electron beam, and eventually the helix turns would touch when the helix tubing diameter became equal to the helix pitch.

The effect of pressure inside the helix will be to raise the boiling temperature of the water in that region, and thus the maximum power capability will be increased for small values of $D_c$, where the power limitation is caused by fluid boiling in the helix. For water the boiling temperature $T_{bw}$ is related to the absolute pressure $p_a$ by

$$T_{bw} = 100 + 32.6 \ln \left(\frac{p_a}{14.7}\right) \text{ in } ^\circ\text{C}, \tag{C13}$$

which is accurate to within about 2°C over the range of absolute pressure from 10 to 140 psi. For a total pressure drop of 50 psi, the average absolute pressure inside the helix is 39.7 psi. Then $T_{bw}$ = 132.4°C, and, for a 20°C inlet temperature, the allowable temperature rise is increased by a factor of (112.4/80), or 1.4. Thus, for small ceramics, the power capability is increased by about 40% as a result of a higher boiling point inside the helix.

### Axial Flow

The axial flow configuration is illustrated in Fig. C5. The measurements of axial flow were made with the flow in the direction indicated in that figure. The optimum direction of fluid flow, however, is such that fluid enters the TWT through the coaxial output window and progresses axially toward the TWT input. The coolant pressure and flow rate decrease with distance toward the input. When the coolant flow rate becomes insufficient for cooling, the cooling system should be terminated and a new one established to cool the circuit toward the input.

When water or other lossy fluid is used as the coolant, the inner diameter of the ceramics should be small, or zero, near the helix output. This is because the fluid is the principal contributor to the RF losses, and they must be minimized near the output for maximum TWT efficiency. The ceramic diameter may be increased toward the helix input without sacrificing efficiency.

The axial flow configuration provides maximum RF power near the circuit output because (a) all of the fluid is used in cooling the helix itself, (b) fluid RF losses in the exit ceramics may be made arbitrarily small, and (c) the fluid pressure, and hence its boiling temperature, is maximum at the output.

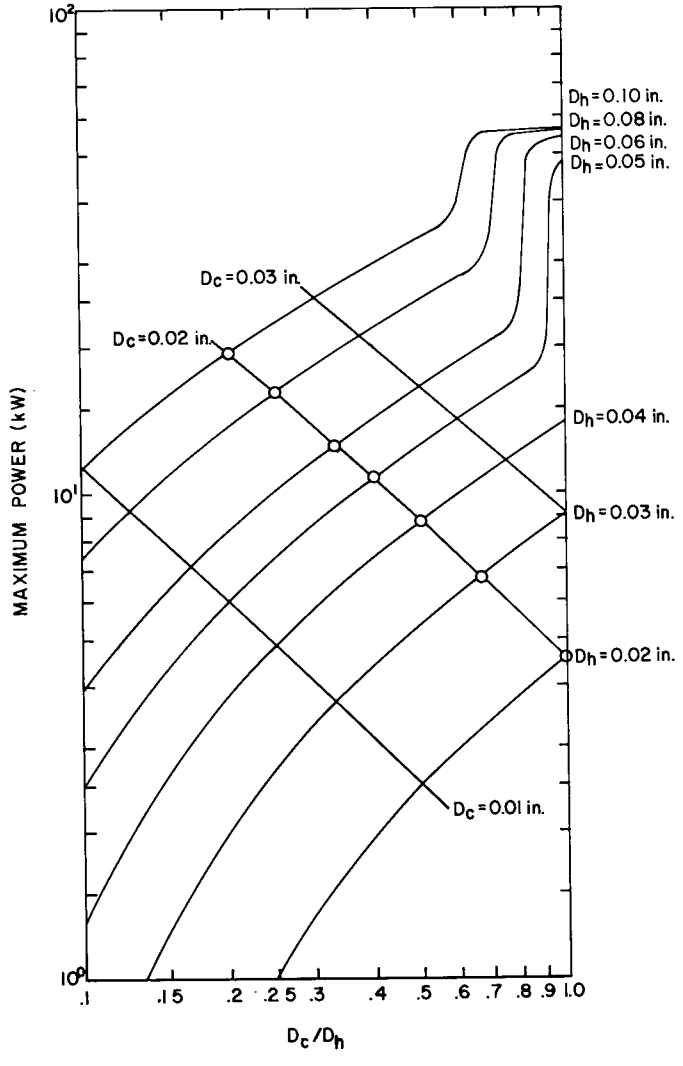


(a)

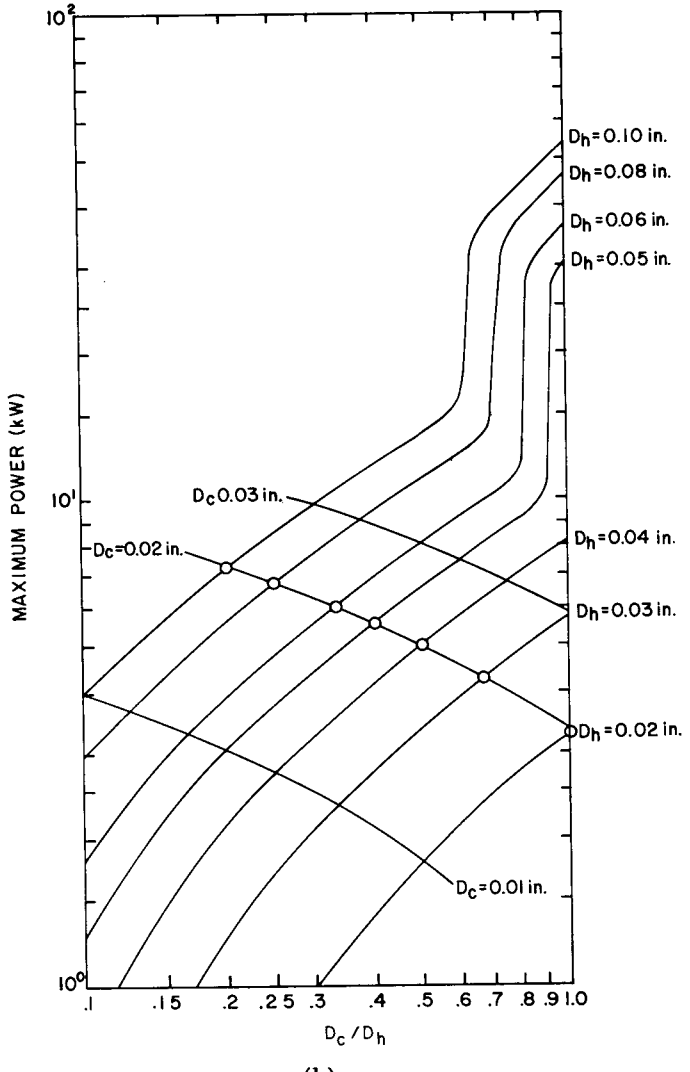


(b)

Fig. C3 — Maximum power computed for cross-flow geometry and water as the coolant for an applied pressure of 50 psi for different helix and ceramic diameters. (a) For 0% beam interception (b) For 2% beam interception (c) For 5% beam interception

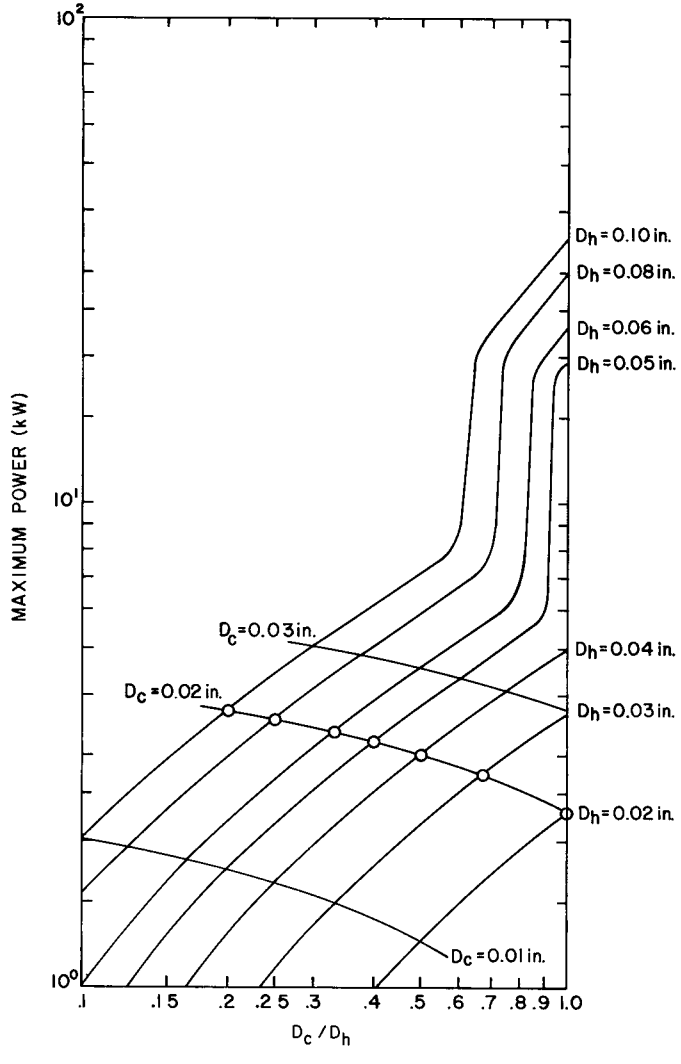


(c)

Fig. C3 — Maximum power computed for cross-flow geometry and water as the coolant for an applied pressure of 50 psi for different helix and ceramic diameters. (a) For 0% beam interception (b) For 2% beam interception (c) For 5% beam interception

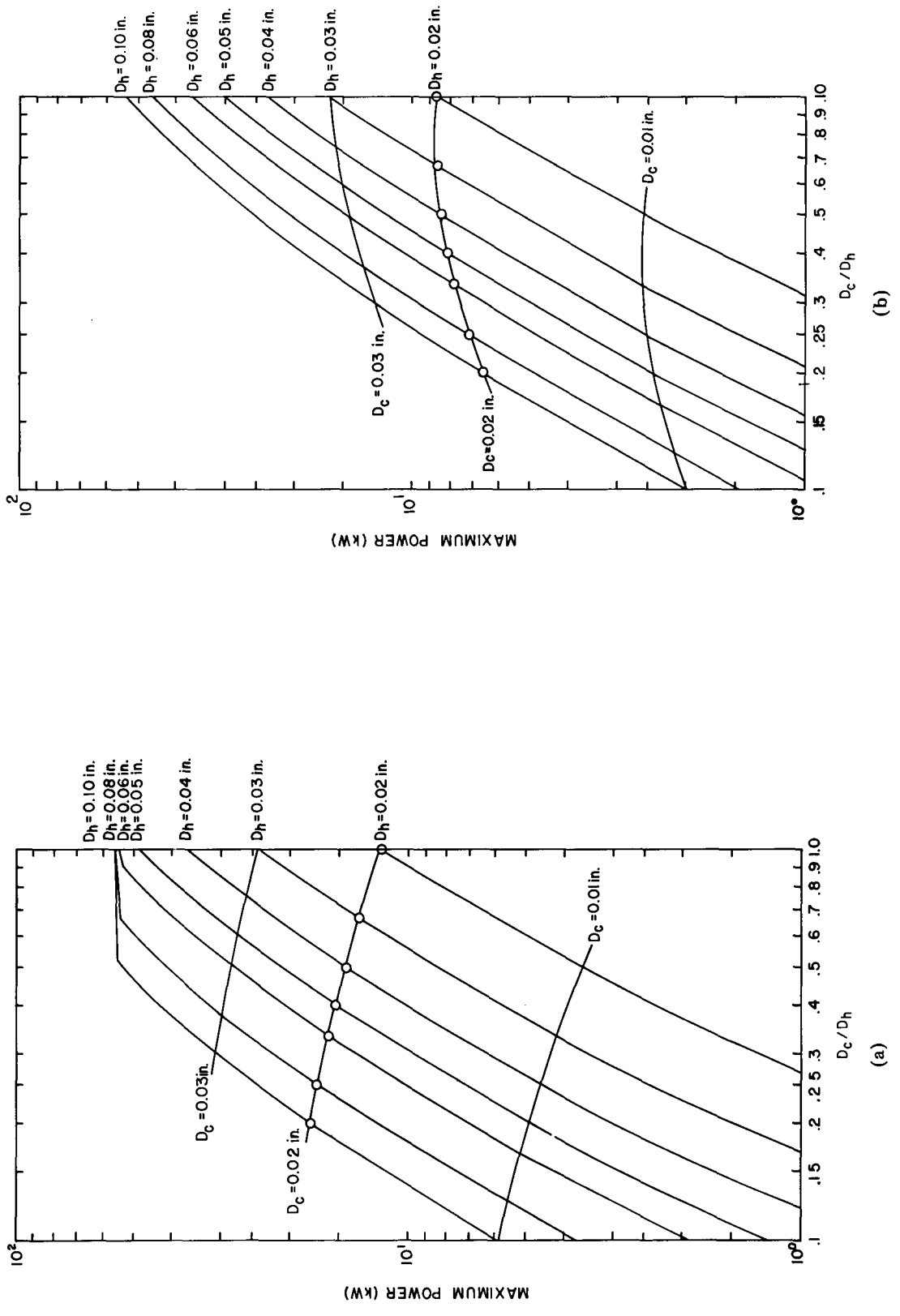


Fig. C4 — Maximum power as in Fig. C-3 except that it is assumed that the fluid flow is turbulent for all values of fluid flow. (a) For 0% beam interception (b) For 2% beam interception (c) For 5% beam interception

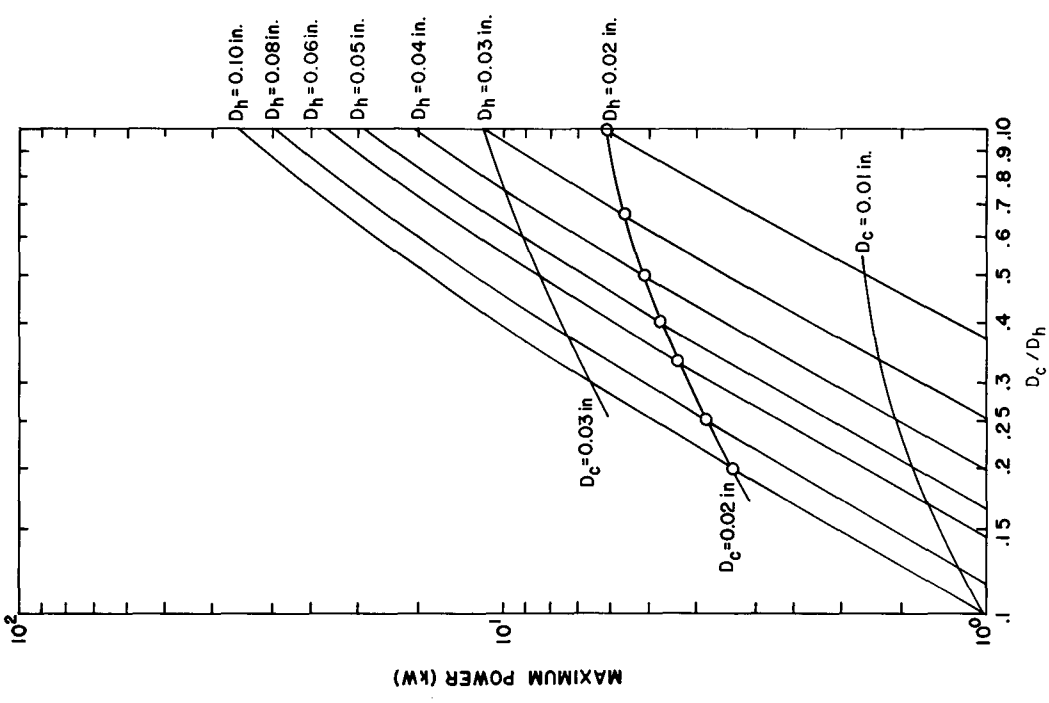


Fig. C4 — Maximum power as in Fig. C-3 except that it is assumed that the fluid flow is turbulent for all values of fluid flow. (a) For 0% beam interception (b) For 2% beam interception (c) For 5% beam interception

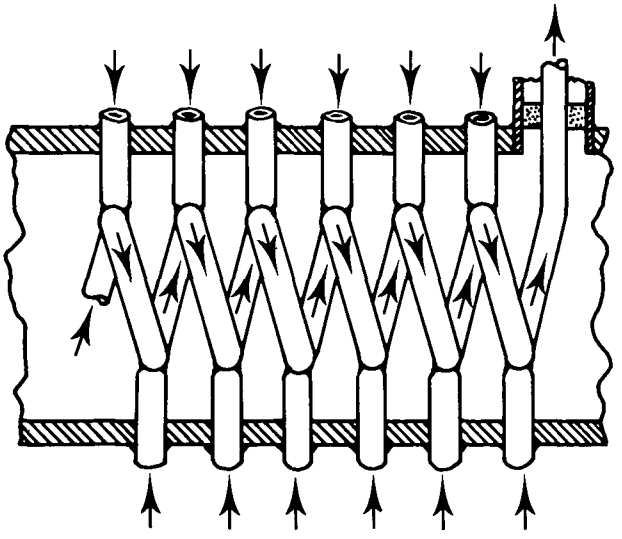

Fig. C5 — Axial flow configuration

The analysis of fluid flow as a function of applied pressure yields results that follow the trend of the experimental measurements, but the computed values of flow are usually high by amounts ranging up to about 15% to 20%. The experimental data were obtained with the direction of flow opposite to that described above as the optimum direction; that is, the measurements were made with the fluid entering through the support ceramics and exiting through the output end of the helix. The flow is assumed to be turbulent inside the support ceramics and either turbulent or laminar inside the helix.

In the analysis the following conventions are adopted:

$p_t$ = the fluid pressure in the input reservoir,

$p_{c(n)}$ = the static pressure in the $n$th ceramic at the point where the fluid enters the helix,

$p_{(n-1)}$ = the static pressure in the helix on the upstream side of the $n$th ceramic,

$F_{c(n)}$ = the flow rate in the $n$th ceramic,

$F_{h(n-1)}$ = the flow rate in the helix on the upstream side of the $n$th ceramic.

Then, from conservation of flow and pressure,

$$F_{h(n)} = F_{h(n-1)} + F_{c(n)} = (1 + r)F_{h(n-1)} \tag{C14}$$

and

$$p_t - p_{(n)} = p_t - p_{(n-1)} + \Delta p_n, \tag{C15}$$

where

$$r = \frac{F_{c(n)}}{F_{h(n-1)}} \,. \tag{C16}$$

As soon as these two equations are coupled by relating $F_c(n)$ to pressure drops and the pressure increment $\Delta p_{(n)}$ to flow rates, and the boundary conditions are established, the problem is formally solved.

Conservation of total power at each junction provides the means of obtaining one of these coupling relations. The total power consists of potential, kinetic, and thermal energy per unit of time components. For the 3-port fluid junction where the fluid from a ceramic enters the helix, the power conservation requirement may be stated as

$$F_{c(n)}\left[p_{c(n)} + \frac{1.124 \times 10^{-3} g F_{c(n)}^2}{D_c^4}\right] + F_{h(n-1)}\left[p_{(n-1)} + \frac{1.124 \times 10^{-3} g F_{h(n-1)}^2}{D_h^4}\right]$$

$$= F_{h(n)}\left[p_{(n)} + \frac{1.124 \times 10^{-3} g F_{h(n)}^2}{D_h^4}\right] + Q_{c(n)} + Q_{(n)}. \tag{C17}$$

Here, $Q_{c(n)}$ is the increase in fluid heat energy per unit time caused by frictional losses as the fluid from the ceramic is mixed with the fluid inside the helix, and $Q_{(n)}$ is the frictional loss that occurs when the fluid in the helix passes by the ceramic and flows through the helix to the next ceramic.

The momentum of the fluid entering the helix from a ceramic is reduced to zero inside the helix. The condition of zero change in the static pressure at the ceramic-helix junction then requires that

$$Q_{c(n)} = \frac{1.124 \times 10^{-3} g F_{c(n)}^3}{D_c^4} \,. \tag{C18}$$

The factor $Q_{(n)}$ results from the pressure drop required to overcome frictional pressure losses between the $(n-1)$th and $n$th ceramics. The first of these frictional pressure losses is that from the fluid flowing through a half turn of helix. This was given in Appendix B as

$$\Delta p_1 = 1.124 \times 10^{-3} C_{B90} C_\theta \frac{g F_{h(n)}^2}{D_h^4}$$

$$\approx 0.32(1+r)^2 \frac{1.124 \times 10^{-3} g F_{h(n-1)}^2}{D_h^4} \,. \tag{B21}$$

The helices used for the axial flow tests were constructed by the taper brazing method described in Appendix A, for which the ceramics penetrate inside the helix wall and cause an obstruction to the helix fluid flow. The pressure drop caused by this obstruction can be described by using Eq. (B25)

$$\Delta p_s = 1.124 \times 10^{-3} C_D \frac{gF^2}{D_2^4} \tag{B25}$$

or in terms of a pressure-loss coefficient $C_V$, as

$$\Delta p_{3_s} = 1.124 \times 10^{-3} C_V \frac{gF_{h(n)}^2}{D_h^4}$$

$$= C_V(1+r)^2 \frac{1.124\, gF_{h(n-1)}^2}{D_h^4} . \tag{C19}$$

From the General Electric Data Books on Heat Transfer, Sec. 405.3, page 1, the value of $C_V$ is taken as

$$C_V = 2.8\left[1 - \left(\frac{A_v}{A_h}\right)^2\right], \tag{C20}$$

where $A_h$ is the helix duct cross-sectional area and $A_v$ is the reduced cross-sectional area of the helix duct at the position of an inlet ceramic. $C_V$ may be combined with $C_{B90}C_\theta$ of Eq. (B21) to give a single loss coefficient $C_L$ given by

$$C_L = 2.8\left[1 - \left(\frac{A_v}{A_h}\right)^2\right] + 0.32 \tag{C20a}$$

and

$$Q_{(n)} = 1.124 \times 10^{-3} C_L (1+r)^3 \frac{gF_{h(n-1)}^3}{D_h^4} . \tag{C20b}$$

If Eqs. (C18) and (C21) are substituted into Eq. (C17) and the assumption is made that

$$p_{c(n)} = p_{(n-1)}, \tag{C22}$$

then the result after rearranging is

$$\Delta p_n = p_{n-1} - p_n = [(1 + C_L)(1+r)^2 - (1+r)^{-1}] \frac{1.124 \times 10^{-3} gF_{h(n-1)}^2}{D_h^4} . \tag{C23}$$

The same assumption (C23) gives from Appendix B

$$p_t - p_{(n-1)} = 1.124 \times 10^{-3} \frac{C_D g F_{c(n)}^2}{D_c^4}$$

$$+ 3.46 \times 10^{-5} (g^{.8} \mu^{.2}) \frac{L_e F_{c(n)}^{1.8}}{D_c^{4.8}} \tag{C24}$$

This equation can be solved exactly for $F_{c(n)}$ in terms of $p_t - p_{(n-1)}$, but since the second term of Eq. (C24) is much smaller than the first term, very little error results if $F_{c(n)}^{1.8}$ is replaced by $F_{c(n)}^2$. With this approximation

$$p_t - p_{(n-1)} = A F_{c(n)}^2$$

or

$$F_{c(n)} = \sqrt{\frac{p_t - p_{(n-1)}}{A}}, \tag{C25}$$

where

$$A = 1.124 \times 10^{-3} \frac{C_D g}{D_c^4} + 3.46 \times 10^{-5} (g^{.8} \mu^{.2}) \frac{L_c}{D_c^{4.8}} \tag{C26}$$

with $C_D$ normally taken as 1.45.

Substituting Eqs. (C16), (C23), and (C25) into Eqs. (C14) and (C16) gives

$$F_{h(n)} = F_{h(n-1)} + \sqrt{\frac{p_t - p_{(n-1)}}{A}} \tag{C27}$$

and

$$p_t - p_{(n)} = p_t - p_{(n-1)} + \frac{1.124 \times 10^{-3} g F_{h(n-1)}^2}{D_h^4} \left[ (1 + C_L) \left( 1 + \frac{\sqrt{\frac{p_t - p_{(n-1)}}{A}}}{F_{h(n-1)}} \right)^2 \right.$$

$$\left. - \left( 1 + \frac{\sqrt{\frac{p_t - p_{n-1}}{A}}}{F_{h(n-1)}} \right)^{-1} \right]. \tag{C28}$$

These are the desired working equations. Once the fluid flow rate and static pressure in the $(n - 1)$th section of helix are known, the corresponding quantities can be computed in the $n$th section of helix. The computation is started by assuming a flow rate in the first ceramic and then proceeding to the output end of the tube where the fluid exits at zero static pressure. The repeated use of Eqs. (C26) and (C27) then yields the final flow at the end of the helix tubing and the value of applied pressure $p_t$ that was needed to produce the assumed initial flow.

The calculated values of $C_L$ based on the helix geometry are

$$C_L \approx 1.56 \text{ for the 0.050-in. I.D. helix}$$

and

$$C_L \approx 1.31 \text{ for the 0.040-in. I.D. helix.}$$

The values of $C_L = 1.31$ compared very favorably with a value of 1.30 which was based on a fluid measurement in which water flowed through a 6-turn length of helix, with the flow in the ceramics blocked. In that case Eq. (C-24) with $r = 0$ gives

$$\Delta p = \frac{1.124 \times 10^{-3} g F_h^2}{D_h^4} (12\, C_L).$$

Unfortunately, a similar measurement was not made to permit verification of the value of $C_L$ calculated for the 0.050-in. I.D. helix.

### Hybrid Flow

The hybrid-flow configuration is illustrated in Fig. C6. The geometry for hybrid flow is similar to that for cross flow, with the exception that the helix tubing is open at the output end of the TWT. Thus fluid flows in one side of the helix and out on the other side, but part of the fluid flows out through the output window, providing much-needed cooling in that region. Because the helix diameter is ordinarily much larger than the ceramic diameter, there is less resistance to flow in the axial direction than through the outlet ceramics. For this reason axial flow will persist for several half turns of the helix, but the flow is eventually transformed to cross flow at a distance from the output.

Very little coolant flows in the helix half turn where the transition from axial flow to cross flow takes place. Therefore if hybrid flow is to be used in cooling high-power TWTs, the hybrid-flow geometry must be such that this low-flow region is far enough away from the output so that severe heating does not occur. This can be accomplished to a certain extent by making a judicious choice of ceramic size relative to the helix tubing size. Another way would be by inhibiting the flow in the outlet ceramics more than in the inlet ceramics. For example, if the butt brazing technique is used, larger holes could be drilled in the helix tubing at the inlet ceramics than at the outlet ceramics.

The analysis of hybrid flow is similar to that presented for axial flow, but now a unit cell must contain two ceramics—one an inlet ceramic and one an outlet ceramic. The general unit cell with terminology is shown in Fig. C7. It has been assumed that the

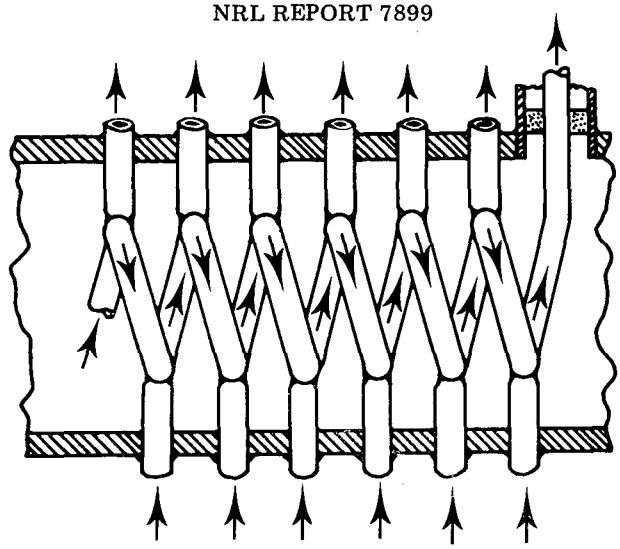

Fig. C6 —Hybrid flow configuration

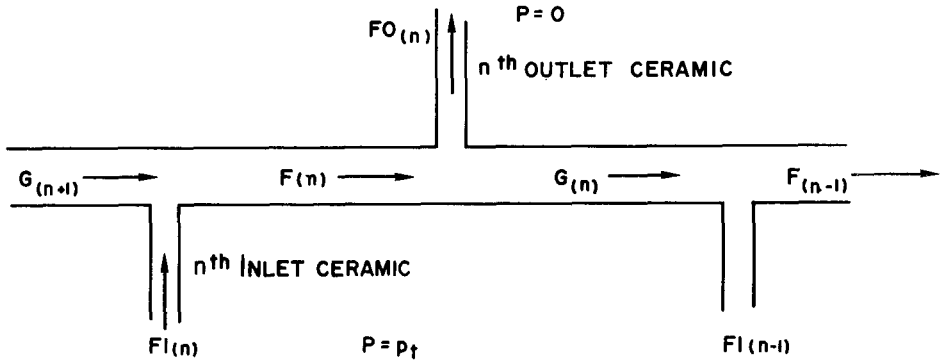


Fig. C7 —Unit cell for hybrid flow

ceramic nearest the output end of the TWT is an inlet ceramic and that the helix is terminated beyond an inlet ceramic. The first unit cell is therefore slightly different than the others, and it will be discussed later in connection with the boundary conditions on the problem.

Two of the equations used in the analysis are the flow rate continuity equations at the outlet ceramics and at the inlet ceramics. These are, respectively,

$$F_{(n)} = FO_{(n)} + G_{(n)} \tag{C29}$$

and

$$F_{(n)} = FI_{(n)} + G_{(n+1)}. \tag{C30}$$

The flow rates are related to pressures in exactly the same way that Eq. (C25) was obtained. The results are

$$FO_{(n)} = \sqrt{\frac{po_{(n)}}{A}} \tag{C31}$$

and

$$FI_{(n)} = \sqrt{\frac{p_t - pI_{(n)}}{A}} \,. \tag{C32}$$

The static pressure increments between ceramics depend on whether the flows $G(n)$ and $G(n + 1)$ are positive or negative;

$$po_{(n)} = pI_{(n-1)} + \frac{1.124 \times 10^{-3} g}{D_h^4} \left[C_L G_{(n)}^2 + (G_{(n)}^2 - F_{(n)}^2)\right] \tag{C33a}$$

if $G_{(n)} > 0$, and

$$po_{(n)} = pI_{(n-1)} - \frac{1.124 \times 10^{-3} g}{D_h^4} (C_L + 1) G_{(n)}^2 \tag{C33b}$$

if $G_{(n)} < 0$.

Likewise,

$$pI_{(n)} = po_{(n)} + \frac{1.124 \times 10^{-3} g}{D_h^4} \left[C_L F_{(n)}^2 + (F_{(n)}^2 - G_{(n+1)}^2)\right] \tag{C34a}$$

if $G_{(n+1)} > 0$, and

$$pI_{(n)} = po_{(n)} + \frac{1.124 \times 10^{-3} g}{D_h^4} (C_L + 1) F_{(n)}^2 \tag{C34b}$$

if $G_{(n+1)} < 0$.

Equations (C28) through (C33) are sufficient to be able to proceed from one unit cell to the next once the solution is started, using the proper boundary conditions. In Eqs. (C32) and (C33), $C_B$ is given by Eq. (B21), and it accounts for the pressure loss in a half turn of the helix. $C_V$ is given by Eq. (C20), and this term accounts for the loss of pressure as the fluid passes the obstacle presented by the tapered ceramics penetrating into the helix. The remaining pressure changes are those produced by acceleration or deceleration of the fluid at the ceramics.

At the first inlet ceramic the situation is that depicted in Fig. C8. The flow boundary condition is

$$F_{(1)} = FI_{(1)} + G_2. \tag{C35}$$

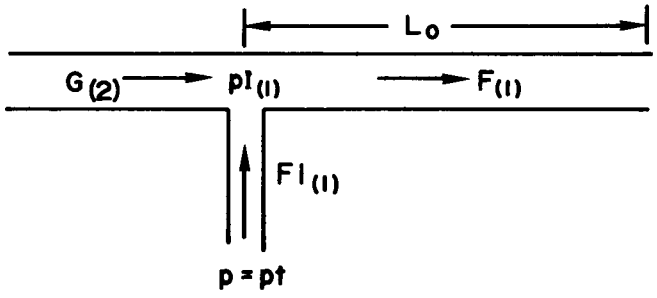


Fig. C8 —Flow conditions at the first inlet ceramic

The flow in the inlet ceramic is given by

$$FI_{(1)} = \sqrt{\frac{p_t - pI_{(1)}}{A}} \tag{C36}$$

The pressure drop in the output section of the helix is related to the flows by

$$pI_{(1)} = \frac{1.124 \times 10^{-3} g}{D_h^4}\left[\frac{L_o}{L_h} C_B F_{(1)}^2 + (F_{(1)}^2 - G_{(12)}^2)\right] \tag{C37a}$$

if $G_2 > 0$ and

$$pI_{(1)} = \frac{1.124 \times 10^{-3} g}{D_h^4}\left(\frac{L_o}{L_h} C_B + 1\right) F_{(1)}^2, \tag{C37b}$$

if $G_2 < 0$.

The computer solution is started by assuming a flow in the first inlet ceramic. One then computes flows and pressures from cell to cell until one reaches the $N$th cell, beyond which the helix is terminated. Therefore one must have in this last cell the condition that

$$FI(N) = F(N). \tag{C38}$$

If an incorrect flow has been assumed in the first ceramic, this condition will not be satisfied, and the process must be iterated until condition (C38) is satisfied.

The process described above has been programmed for a high-speed computer. As might be expected, the flow from the output end of the helix is rather sensitive to the output length $L_o$. When the experiments on hybrid flow for the S-band TWT were performed, the value of $L_o$ was not recorded. A value of 1 in. for $L_o$ yields almost exact agreement with the experiment for the case of $D_c$ = 0.020 in., $D_h$ = 0.040 in. The same value of $L_o$, however, gives end flow of about 0.2 gpm, compared to the measured value of 0.137 gpm for the case of $D_c$ = 0.032 in., $D_h$ = 0.050 in.

## LIST OF SYMBOLS

The symbols that are used in this report are usually defined, together with their dimensions, the first time they appear. They are tabulated here for reference purposes.

| | |
|---|---|
| $A$ | fluid flow coefficient, defined by Eq. (C27) |
| $A_h$ | cross-sectional area of helix duct (in.$^2$) |
| $A_v$ | cross-sectional area of flow obstruction (in.$^2$) |
| $a$ | helix radius (in.) |
| $b$ | Pierce's normalized TWT synchronism parameter |
| $C$ | Pierce's normalized TWT gain parameter |
| $C_B$ | flow resistance coefficient for a half turn of helix ($C_{B90}C_\theta$) for $\theta = 180°$ (dimensionless) |
| $C_{B90}$ | flow resistance coefficient for a 90° bend (dimensionless) |
| $C_D$ | flow resistance coefficient (dimensionless) |
| $C_L$ | $C_V + C_B$ |
| $C_V$ | flow resistance coefficient for an abrupt obstruction (dimensionless) |
| $C_\theta$ | factor by which $C_{B90}$ is multiplied to give resistance factor for a bend angle $\theta$ (dimensionless) |
| $c$ | specific heat (Btu/lb °F) |
| $D$ | fluid duct diameter (in.) |
| $D'$ | fluid duct diameter (ft) |
| $D_c$ | ceramic duct diameter (in.) |
| $D_h$ | helix duct diameter (in.) |
| $d$ | Pierce's normalized TWT loss parameter for the forward wave |
| $d_{-1}$ | Pierce's normalized TWT loss parameter for the backward wave |
| $E$ | electric potential (V) |
| $E_h$ | helix potential (V) |
| $F$ | fluid flow rate (gpm) |

| | |
|---|---|
| $F'$ | fluid flow rate ($ft^3$/hr) |
| $F_c$ | fluid flow rate in ceramic for cross flow (gpm) |
| $F_{c(n)}$ | fluid flow rate in the $n$th ceramic in axial flow (gpm) |
| $F_h$ | fluid flow rate in helix for cross flow (gpm) |
| $F_{h(n)}$ | fluid flow rate in the helix on the downstream side of the $n$th ceramic in axial flow (gpm) |
| $FI_{(n)}$ | fluid flow rate in the $n$th inlet ceramic in hybrid flow (gpm) |
| $F_{(n)}$ | fluid flow rate in the helix in the upstream section at the $n$th outlet ceramic in hybrid flow (gpm) |
| $FO_{(n)}$ | fluid flow rate in the $n$th outlet ceramic in hybrid flow (gpm) |
| $F_T$ | fluid flow rate at the transition between laminar and turbulent flow (gpm) |
| $f$ | friction factor (dimensionless) |
| $G_{(n)}$ | fluid flow rate in the helix in the section adjacent to the $n$th outlet ceramic on the side toward the output (gpm); hybrid flow |
| $g$ | specific gravity relative to water at 4°C (dimensionless) |
| $g_c$ | acceleration of gravity (assumed to be 32.14 ft/$sec^2$) |
| $I$ | electric current (A) |
| $I_b$ | electron beam current (A) |
| $\Delta I_h$ | increase in helix intercepted beam current because of RF drive (A) |
| $K_c$ | contraction loss coefficient (dimensionless) |
| $K_e$ | expansion loss coefficient (dimensionless) |
| $k$ | thermal conductivity (Btu/hr ft °F) |
| $k_b$ | dimensionless coefficient used in Eq. (B9) |
| $L$ | length (in.) |
| $L'$ | length (ft) |
| $L_c$ | length of ceramic support (in.) |
| $L_h$ | length of a half turn of helix (in.) |

$L_o$ output length of helix (in.)

$m$ mass (lb)

$N$ total number of turns of helix

$n$ index number used in axial and hybrid flow analysis

$P$ power (W)

$P'$ power (ft-lb/hr)

$P_b$ DC power carried by the electron beam (W)

$P_c$ RF power dissipated in fluid in ceramic (W)

$P_F$ RF power traveling toward the output (W)

$P_h$ RF power dissipated at helix per half turn (W)

$P_i$ power dissipated on the TWT circuit because of electron beam interception (W)

$P_o$ output RF power (W)

$P_R$ reflected RF power (W)

$P_{RF}$ peak RF power (W)

$P_t$ thermal power (W)

$p$ pressure (psi)

$p'$ pressure ($lb/ft^2$)

$p_a$ absolute pressure (psi)

$p_{c(n)}$ static pressure in the $n$th ceramic at the point where the fluid enters the helix, in axial flow (psi)

$pI_{(n)}$ static pressure in the $n$th inlet ceramic at the point where it enters the helix, in hybrid flow (psi)

$p_{(n)}$ static pressure in the helix on the downstream side of the $n$th ceramic, in axial flow (psi)

$po_{(n)}$ static pressure at the $n$th outlet ceramic at the point where it enters that ceramic, in hybrid flow (psi)

$p_t$ total applied pressure (psi)

| | |
|---|---|
| $Q$ | quantity of heat energy (Btu) |
| $Q_{(n)}$ | frictional fluid loss term in axial flow (cf. Eq. (C17)) |
| $Q_{c(n)}$ | frictional fluid loss term in axial flow (cf. Eq. (C17)) |
| $R_D$ | Reynolds number for fluid flowing in a duct (dimensionless) |
| $r$ | voltage reflection coefficient (dimensionless) |
| $r$ | dimensionless coefficient defined by Eq. (C16) |
| $T$ | temperature (°C) |
| $T'$ | temperature (°F) |
| $T_{ba}$ | boiling temperature of water (°C) |
| $T_i$ | inlet temperature (°C) |
| $\Delta T_c$ | change in fluid temperature while flowing through ceramic (°C) |
| $\Delta T_D$ | temperature difference between helix surface and fulk of fluid in helix (°C) |
| $\Delta T_h$ | change in fluid temperature due to electron-beam interception and RF power dissipation in a half turn of helix (°C) |
| $V'$ | average fluid velocity (ft/sec) |
| $VH$ | velocity head (psi) |
| $\mu$ | absolute viscosity (lb/ft-hr) |
| $\rho$ | fluid density ($lb/ft^3$) |
| $\tau$ | RF loss (dB) |
| $\tau_c$ | RF loss in the fluid of a ceramic support (dB) |
| $\tau_h$ | RF loss in a half turn of helix (dB) |